Thin-Walled Structures 169 (2021) 108448

Contents lists available at ScienceDirect

Thin-Walled Structures

journal homepage: www.elsevier.com/locate/tws

Full length article

Postbuckling mechanics in slender steel plates under pure shear: A focus on boundary conditions and load path

Peter Y. Wang [a], Parfait M. Masungi [a], Maria E.M. Garlock [a,*], Spencer E. Quiel [b]

[a] *Princeton University, Department of Civil and Environmental Engineering, 54 Olden Street, Princeton, NJ 08544, USA*

[b] *Lehigh University, Department of Civil and Environmental Engineering, Fritz Engineering Laboratory, 13 East Packer Avenue, Bethlehem, PA 18015-3176, USA*

A R T I C L E I N F O

Keywords:
Shear buckling
Boundary condition
Postbuckling
Plate girder
Load path
Thin steel plate

A B S T R A C T

Slender steel plates used in buildings, bridges, aircraft, and ships have postbuckling shear strength that is mobilized in design. Despite a century of research on this topic, the mechanics (load path and failure mechanisms) of the postbuckling behavior are still not fully understood. Proper boundary conditions are vital for studying the mechanics in finite element (FE) models, yet several different boundary conditions have been proposed by researchers. This paper uses FE models to examine various boundary conditions on a slender plate under pure shear loading. The models are benchmarked against 16 experimental tests, with a range of web depths (D), panel aspect ratios, and web slenderness ratios. The effects of boundary conditions on the normal stresses on the web plate edges and principal stresses in the web are examined for panel aspect ratios of 1, 2, and 3. The flanges, stiffeners, and "panel extensions" (which extend the web and flange a distance $D/2$ beyond the stiffener on either side of the panel) are used as boundary conditions (with axially free vertical edges at the ends of the panel). The analysis results show negligible participation from the stiffeners and flanges in the load path up to the ultimate postbuckling shear load, while compressive membrane stresses in the web are observed to redistribute and continue to increase after elastic buckling, in some regions at a greater rate than before buckling. This study advances the understanding of postbuckling shear load path that can be used in code development and performance enhancements for shear buckling in slender plates.

1. Introduction

Deep beams in buildings and bridges, shear walls, aircraft, and ship hulls commonly use thin steel plates to achieve their design strength. To satisfy load demands and deflection criteria, it is efficient for these structures to maximize plate depth and minimize plate thickness, resulting in slender web plates. Slender web plates are susceptible to web shear buckling; however, they have significant additional strength beyond elastic buckling that was first documented by Wilson in 1886 [1] and theorized by researchers such as Wagner in aeronautical design [2]. To ignore this postbuckling strength would be very conservative, so the ultimate postbuckling shear capacity (V_u) is utilized in structural engineering design codes today [3–5]. A brief introduction follows, though detailed literature reviews of web shear buckling research have been compiled by [6] and more recently by [7].

The first postbuckling shear strength theory was proposed by Wagner in 1931 for aeronautical structures and recognized the development of diagonal tension after elastic buckling in thin metal plates [2]. In early days, though postbuckling strength was observed, the elastic buckling load was still used as the basis for design shear strength since no theory was available to precisely quantify the postbuckling strength [8,9]. In the 1960s, Konrad Basler developed the first semi-empirical design equations predicting ultimate postbuckling shear strength of steel plates in civil engineering structures [9,10]. These equations were proposed based on a set of experimental tests on transversely stiffened steel plate girders, which were used to develop the now widely known Tension Field Action (TFA) theory. Tension Field Action holds that compressive stresses cease to increase after elastic buckling, and instead additional load is sustained by a "tension field" in the web, which is vertically anchored by transverse stiffeners. TFA theory operates under the Pratt truss assumption, which assumes that load travels up the tension field like the diagonals of a Pratt truss and down the vertical (transverse) stiffeners in axial compression. TFA theory uses the von Mises yield criterion to predict the ultimate postbuckling shear load V_u of plate girder webs. TFA ignores any contribution from the flanges, which it deemed "too flexible" to be able to anchor the tension field. As such, this theory was both easy to use and relatively accurate in its strength predictions [6]. TFA theory was adopted by AISC shortly after its publication in 1963 as well as by AASHTO in 1973 [3,4,11].

* Corresponding author.
E-mail addresses: pywang@alumni.princeton.edu (P.Y. Wang), pmasungi@princeton.edu (P.M. Masungi), mgarlock@princeton.edu (M.E.M. Garlock), seq213@lehigh.edu (S.E. Quiel).

https://doi.org/10.1016/j.tws.2021.108448
Received 3 February 2021; Received in revised form 10 September 2021; Accepted 12 September 2021
Available online xxxx

Over time, several researchers have proposed revisions to Basler's theory [12–14]. A host of other tension field theories and models followed, including the Cardiff model (Porter et al. [15]) and Torsten Höglund's "Rotated Stress Field Theory" [16] which claims that unstiffened girder panels (where the web panel length exceeds three times the web depth) can still develop postbuckling shear strength; this theory has been adapted for use in several current design specifications [4,5,17]. However, all of these theories are tension field theories and operate off the same central assumption: that compression stresses cease to increase after elastic shear buckling and any additional strength is via a tension field sustaining further load beyond elastic buckling [6]. New studies have shown, however, that compressive stresses can increase significantly after elastic buckling in the perimeters of the web plate [18–20].

Recent research has found that several of the assumptions used in TFA theory are not necessarily accurate. Advances in finite element modeling and experimental testing have allowed researchers to track the flow of forces (i.e., load path) in the postbuckling shear regime. Both experimental [21,22] and finite element research [23–25] have shown that the transverse stiffeners are not primarily loaded in axial compression to anchor the tension field; instead they are engaged primarily in out-of-plane bending to laterally restrain the edges of the panel as it buckles and subsequently deforms [26]. As a result, prominent design specifications such as AISC and AASHTO have removed the area requirement of transverse stiffeners, which are no longer perceived to carry substantial axial load [3,4]. These developments point towards an incomplete load path in Basler's TFA theory.

Regarding the flanges, Yoo and Lee have suggested that the flanges' primary contribution to shear capacity is to the elastic shear buckling load V_{cr} (by providing rotational restraint at the top and bottom edges of the web plate), rather than increasing the postbuckling shear reserve ($V_u - V_{cr}$) [11,18]. The flanges also have an implicit role in maintaining an out-of-plane restraint up to the ultimate postbuckling shear load V_u, which may be related to the flange-to-web stiffness ratio [27]. Other authors [6] have observed that the formation of plastic hinges in the flanges can occur after reaching maximum shear load, suggesting that the flange hinges may not be critical in determining the ultimate strength. For example, Scandella et al. suggest that the flanges' strength contribution to the postbuckling shear reserve only occurs after V_u (the first and highest peak in the load–displacement curve) [28]. Following V_u, the plate girder unloads, after which there is a stiffness recovery associated with flange bending and a secondary peak is reached at flange hinging which may not exceed the first peak load V_u [28].

Various boundary conditions have been used to study web shear buckling [11,18–20,29]. Some authors modeled the edges of the web as simple supports [18–20,29], while others explicitly modeled the flanges and/or stiffeners [11,18,19]. Further, some authors longitudinally restrained the web panels [20,25,29], while others modeled the panels as longitudinally free [11,18]. Lee et al. [30] evaluated the effects of rigid anchors and beam elements at the top and bottom edges of the plate (in place of flanges) to study the effects of potential flange anchoring mechanisms. To examine the load path of tensile and compressive forces in a plate subject to shear, it is important to use appropriate boundary conditions, yet it is not clear which boundary condition is the most precise.

This paper presents a comprehensive examination on the effects of various boundary conditions on a steel plate subject to pure shear loads. These boundary conditions represent the flange (horizontal) edge and the stiffener (vertical) edge with the intent of capturing the true behavior (strength and stress distribution) of a stiffened panel in a steel plate girder. The objective of this work is to (1) identify appropriate boundary conditions that capture both the ultimate postbuckling shear strength and load path (flow of forces), and (2) examine the load path of tensile and compressive membrane stresses to enable a better understanding of the postbuckling behavior of slender steel plates under pure shear loads.

2. Finite element model

A nonlinear finite element (FE) study was conducted in ABAQUS 2017 [31] to investigate the elastic buckling and postbuckling behavior of slender steel plates loaded in pure shear. For all analyses, four-node "S4" shell elements ("doubly-curved, general purpose, finite membrane strains") were used [31], with 5 section points through each plate's thickness [20] . The material model for mild steel was elastoplastic with strain hardening [32,33], defined for ambient temperatures by Eurocode 3 Part 1–2 [5]. The steel yield stress F_y and Young's modulus E will be specified for each girder specimen in the study, and the Poisson's ratio was taken as 0.3 for all models. The mesh density used in each of the analyses was determined by a convergence study on the elastic shear buckling load V_{cr}, of a simply supported steel plate, converging within 2.5% of Timoshenko's shear buckling load given in Eq. (1) [34]. Eq. (1) represents V_{cr}, with the associated buckling coefficient values computed from Eq. (2).

$$V_{cr} = Dt_w * \frac{k\pi^2 E}{12\left(1-\mu^2\right)(D/t_w)^2} \tag{1}$$

$$k = 5.34 + \frac{4.00}{(a/D)^2} \qquad for\ a/D \geq 1.0 \tag{2}$$

Fig. 1 shows the typical mesh density and various boundary conditions used in four of the plate panel models. Five through-thickness section points was determined to be adequate via a convergence study on principal stresses on the surfaces of the web plate for the authors' previous work [20].

A linear elastic eigenvalue analysis was first conducted for each specimen to determine its elastic shear buckling load eigenvalue V_{cr} and the specimen's buckled eigenmodes. For the subsequent incremental analysis, a scaled initial geometric imperfection of the first positive buckled eigenmode was overlaid onto the specimen's finite element mesh; this allows the analysis to proceed past the elastic buckling bifurcation and simulates the influence of realistic geometric imperfections [29,32,35]. The magnitude of the scaled imperfection equals $D/1000$ unless otherwise noted, where D is the web depth. A discussion of the influence of imperfection magnitude is provided in Sections 3.4 and 4.2.2. Nonlinear incremental analysis is performed via the Modified Riks algorithm to quasi-statically load the specimen to failure. The ultimate postbuckling shear load V_u was determined as the maximum load in the load–displacement curve, where the displacement is measured as the relative vertical displacement between the top left and bottom right corners of the center panel. Since the influence of panel boundary conditions is a major objective of this research, a description of the boundary conditions will be provided in Section 3 along with the validation of the finite element model.

The S4 elements used in the FE solutions consider both membrane and bending stresses through the thickness of the plate, t. ABAQUS outputs stresses (S), at all integration points through the depth; integration of the stresses through the thickness creates the section force, which when divided by the thickness gives the membrane stress. The authors have previously shown that second order bending stresses in the buckled web plate play a substantial role in the stress state at V_u [20]. However, membrane stresses are more useful in analyzing the flow of forces (i.e., load path) in a plate since their resultant is not influenced by through-thickness bending actions. For example, Fig. 2 illustrates the difference between membrane stress (σ_{m}) and stress at the center of thickness ($\sigma_{\mathrm{t/2}}$). If the material remains elastic through the plate thickness, the membrane stress at this stage (σ_{m1}) is equal to $\sigma_{\mathrm{t/2}}$ as shown in Fig. 2(a). However, when the bending in the plate increases to yield as shown in Fig. 2(b), the membrane stress at this stage (σ_{m2}) becomes smaller than $\sigma_{\mathrm{t/2}}$. Since the stress distribution through the thickness is 'cut-off' by the yield capacity of the material (i.e., the dashed red line in Fig. 2(b)), integrating the stresses through the depth and dividing it by the thickness would produce a stress resultant lower than that acting at mid-depth. It has been shown previously [20] that

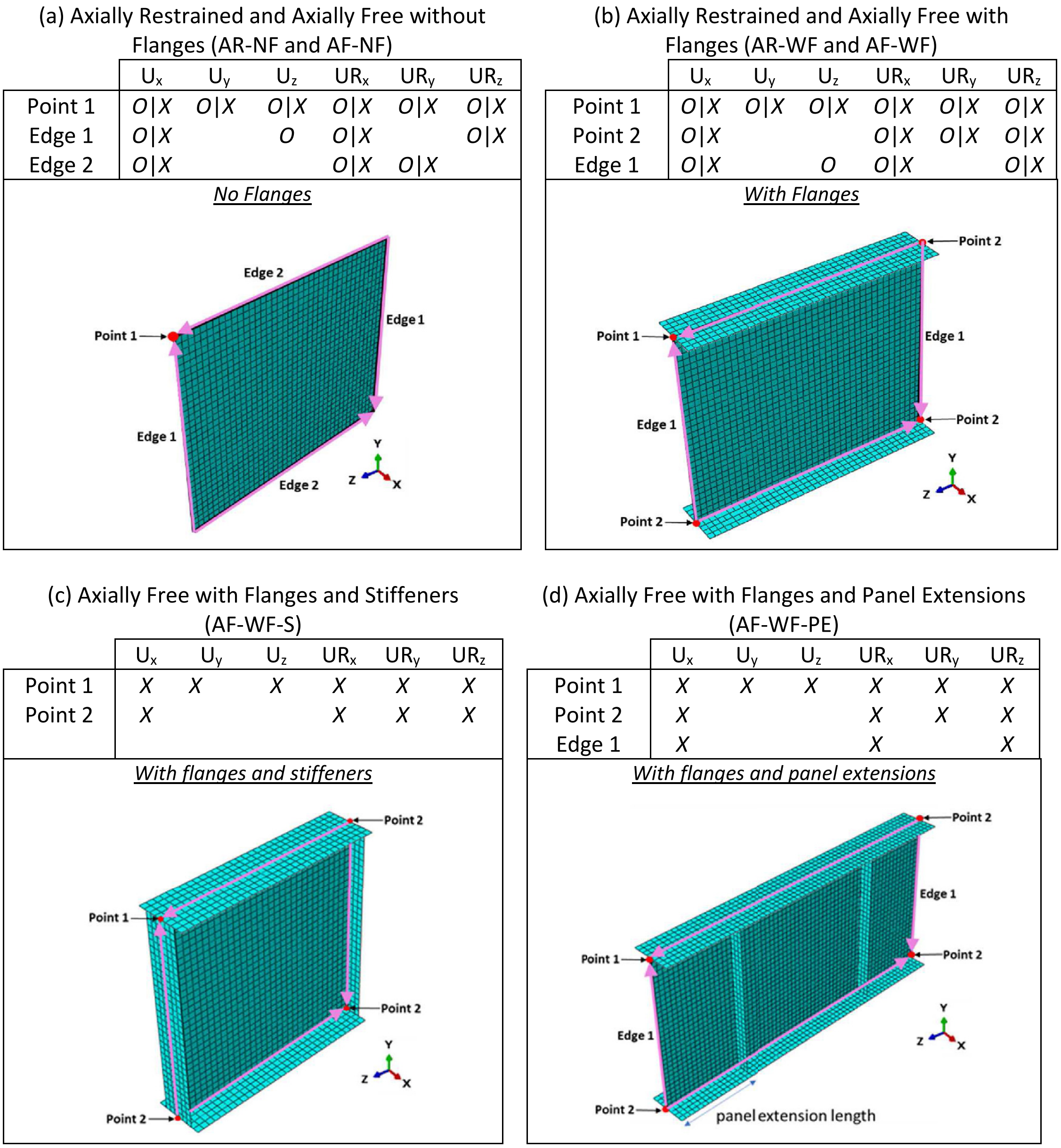

(a) Axially Restrained and Axially Free without Flanges (AR-NF and AF-NF)

	U_x	U_y	U_z	UR_x	UR_y	UR_z
Point 1	$O \mid X$	$O \mid X$	$O \mid X$	$O \mid X$	$O \mid X$	$O \mid X$
Edge 1	$O \mid X$		O	$O \mid X$		$O \mid X$
Edge 2	$O \mid X$			$O \mid X$	$O \mid X$	

(b) Axially Restrained and Axially Free with Flanges (AR-WF and AF-WF)

	U_x	U_y	U_z	UR_x	UR_y	UR_z
Point 1	$O \mid X$	$O \mid X$	$O \mid X$	$O \mid X$	$O \mid X$	$O \mid X$
Point 2	$O \mid X$			$O \mid X$	$O \mid X$	$O \mid X$
Edge 1	$O \mid X$		O	$O \mid X$		$O \mid X$

(c) Axially Free with Flanges and Stiffeners (AF-WF-S)

	U_x	U_y	U_z	UR_x	UR_y	UR_z
Point 1	X	X	X	X	X	X
Point 2	X			X	X	X

(d) Axially Free with Flanges and Panel Extensions (AF-WF-PE)

	U_x	U_y	U_z	UR_x	UR_y	UR_z
Point 1	X	X	X	X	X	X
Point 2	X			X	X	X
Edge 1	X			X		X

Fig. 1. Boundary conditions imposed on models (a), (b), (c), and (d) which indicate translational (U) and rotational (UR) restraint. Axially restrained boundary conditions are represented by (O) and axially free boundary conditions are represented by (X). Pink arrows represent shear edge loading. (For interpretation of the references to color in this figure caption, the reader is referred to the web version of this article.)

the plate does not remain elastic through the thickness before reaching V_u, and significant bending develops through the plate thickness as the buckled plate continues to deform. For this reason, the membrane stresses are used in this paper for determining load path (as done by others, including [18,36]).

3. Boundary condition study

The ultimate goal of this research effort is to understand the mechanics that lead to web shear buckling. To enable this discovery, finite element models must be developed to capture both the ultimate postbuckling shear strength (V_u) and path of membrane forces. This section seeks to identify such models by examining various boundary conditions on the web panel of interest (i.e., with various lateral, longitudinal, and rotational restraints, as well as explicit modeling of flanges and stiffeners) and initial imperfections. The models' results are compared to a suite of experimental data for validation.

3.1. Boundary condition parameters

The boundary conditions used in this study are presented in Fig. 1, starting from a simply supported plate onto which girder components such as flanges and stiffeners are incrementally added. For all boundary conditions, uniformly distributed shear loads are applied along the four edges of the web plate. The nomenclature representing the boundary conditions is the following:

- AR/AF = Axially Restrained or Axially Free, specifically referring to whether the plates are longitudinally restrained or free at the vertical ends of the web
- NF/WF = No Flange or With Flange
- S = Stiffener model, which always has flanges (WF) and is always axially free (AF)
- PE = Panel Extension model, which always has flanges (WF) and stiffeners and is always axially free (AF).

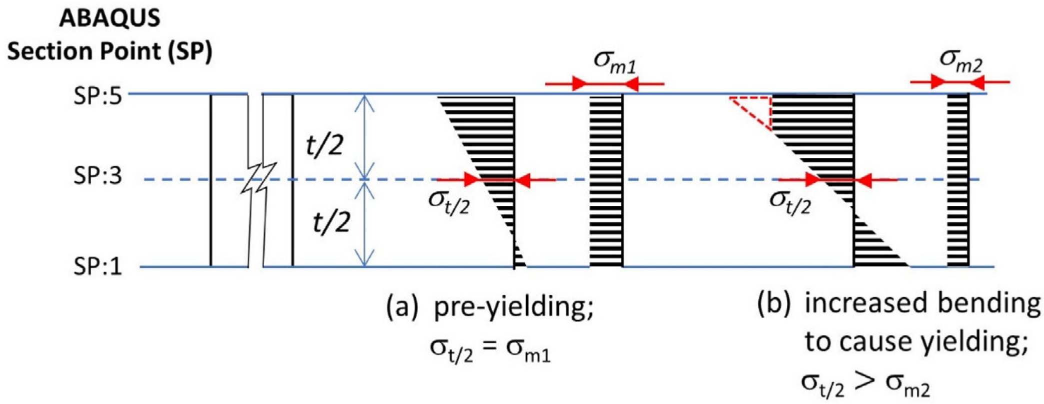

Fig. 2. Illustration of the difference between the membrane stress (σ_m) and the stress at the plate center thickness ($\sigma_{t/2}$) (a) pre-yielding (no difference) and (b) with some yielding induced by increased bending.

In the PE models, the panel extension is defined as the distance between the centerline of the stiffener to the end of the panel extension (see Fig. 1(d)). Note that the panel extensions end in virtual stiffeners (i.e., Edge 1 in Fig. 1(d) has an out-of-plane translational restraint), and preliminary models that explicitly include these stiffeners produced the same elastic shear buckling and ultimate postbuckling shear strength results. The current work also includes the longitudinal boundary conditions imposed on the vertical edges of the web plate as a parameter of the experimental validation: axially free (AF) or axially restrained (AR), where the latter indicates that horizontal reactions at the left and right edges of the web do not permit longitudinal translation. AF is a lower bound on the longitudinal restraint that would be available to a girder panel (note that AF-NF was used by [18]). AR is an upper bound which also implicitly assumes the availability of infinite horizontal reaction capacity at the vertical ends of the web panel. The models with stiffeners only (WF-S) and with panel extensions (WF-PE) were only studied with axially free boundary conditions. A state of pure shear in the elements was observed prior to elastic buckling, thus validating the elastic response. The inelastic response was validated with experimental data as discussed in the next subsection.

3.2. Experimental validation

Finite element (FE) models with the various boundary conditions in Fig. 1 were compared to a set of 16 experimental tests completed by various researchers and compiled by [29]. Table 1 summarizes the dimensions and material properties of the test specimens selected for validation. For the dimensions in Table 1, D represents the web depth, t_w is the web thickness, a is the horizontal panel length (distance between stiffeners in the specimen), b_f is the flange width, t_f is the flange thickness, b_s is the stiffener width, and t_s is the stiffener thickness. To make sure the modeling is robust for a range of geometries, the selected specimens have a wide range of web depths (D), slenderness ratios (from $D/t_w = 100$ to 302), and web panel aspect ratios (from $a/D = 1$ to 3). An assumed initial geometric imperfection magnitude of $D/1000$ was used in all validation models, which is on the order of measurements made on bridge girder webs in a steel shop [37] and used in previous work [18,32].

Five boundary conditions are studied and compared in the experimental validation study, using the nomenclature described earlier: AR-NF [20,29], AF-NF [18], AR-WF [19], AF-WF [18], [19], and AF-WF-PE (see Fig. 1). Note that the panel extension lengths for the PE models are set equal to either $D/10$ (which is the minimum length requirement for rigid end posts in the Eurocode [35]) or $D/2$ (see Fig. 1(d)) to examine sensitivity to panel continuity. Preliminary analyses showed that panel extension lengths longer than $D/2$ did not appreciably affect the calculated values of V_{cr} or V_u. The purpose of studying various panel extensions was to determine the best correlations with experimental results (to calculate shear strength), while also capturing the true response of compressive and tensile force load path in a continuous girder (i.e., not just an isolated plate) where the web panel is defined by stiffener placement.

The AR-NF columns of Table 2 summarize the results of models with boundary conditions that are axially restrained with no flanges, as shown in Fig. 1(a). It is observed that for most specimens, the FE results predict the ultimate postbuckling shear load ($V_{u.FE}$) within 10% for most models when compared with the published experimental results ($V_{u.Exp}$). In contrast the AF-NF models, which free the axial restraint and assume zero horizontal reactions on the left and right web edges, gave noticeably low estimations of the ultimate postbuckling shear load V_u when compared with experiments. As the lower bound solution, the V_u values predicted by the AF-NF models were typically about 65% of the experimental V_u values. Though not shown, the elastic shear buckling loads (V_{cr}) of the AF-NF models were identical to the V_{cr} values of the AR-NF models (as noted by the authors in [19]); therefore, the lower V_u values of the AF-NF models come from the decrease in their postbuckling reserve $V_u - V_{cr}$ when axial restraint is freed at the web edges. It is thus concluded that the horizontal reactions at the locations of axial restraint (i.e., at the left and right vertical edges of the web panel) play a role in how much postbuckling reserve can be achieved.

By comparing the FE results of AR-NF and AF-NF to the models that explicitly model the flanges (models AR-WF and AF-WF, respectively), it is seen that modeling the flanges raises the FE V_u values. With flanges, the axially restrained AR-WF models over-predict the experimental V_u values by 10% on average. Meanwhile, the axially free with flanges models (AF-WF) still underpredict experimental V_u values by 16% on average, suggesting they may still be lacking a component of the load path in the postbuckling mechanics of the experimental specimens.

It is shown that both the panel extension model (AF-WF-PE) with panel extension length $D/2$ and AR-NF models have the best correlation to the experimental results, with an average $V_{u.FE}/V_{u.Exp}$ ratio of 0.997 and 1.008, respectively. While both capture V_u well, only AF-WF-PE with panel extension length $D/2$ captures the path of membrane forces properly, as will be shown in Section 4.2. Therefore, this model will be used to develop the prototype described next.

3.3. Girder prototype and influence of girder components

The experimental data presented previously were based on specimens with slenderness ratios (D/t_w) typically greater than 200. Current design practice usually uses plates with smaller slenderness ratios; for example, the AASHTO bridge design code restricts transversely stiffened and unstiffened webs to a slenderness less than or equal to 150 [3]. The numerical study in this section and in sections to

Table 1
Geometric and material properties considered for FE model validation.

Specimen	a (mm)	D (mm)	t_w (mm)	a/D	D/t_w	t_f (mm)	b_f (mm)	b_s[a] (mm)	F_y (MPa)	E (GPa)
G6-T1 [9]	1905	1270	4.90	1.50	259	19.80	308	101.60	250	210
G7-T1 [9][b]	1270	1270	4.98	1.00	255	19.53	310	101.60	250	210
G7-T2 [9][b]	1270	1270	4.98	1.00	255	19.53	310	101.60	250	210
G8-T1 [9]	3810	1270	5.08	3.00	250	19.10	305	101.60	263	210
G8-T2 [9][b]	1905	1270	5.08	1.50	250	19.10	305	101.60	263	210
G8-T3 [9][b]	1905	1270	5.08	1.50	250	19.10	305	101.60	263	210
2.2 [38]	1464	600	2.00	2.40	300	6.00	175	63.50	250	210
US3/5 [39]	788	359	2.70	2.19	133	12.00	96	38.10	250	210
STG1 [40]	551	279	2.00	1.97	140	7.90	127	50.80	250	210
STG4 [40]	498	251	1.25	1.98	201	6.40	102	38.10	250	210
RTG1 [40]	305	305	1.27	1.00	240	4.50	76	31.75	261	210
RTG2 [40]	305	305	1.27	1.00	240	4.70	76	31.75	261	210
MSO [41]	947	608	2.01	1.56	302	10.10	102	41.91	261	210
CP1/1 [42]	747	500	2.04	1.49	245	8.00	100	38.10	250	210
S-2 [43]	581	319	3.20	1.82	100	10.50	100	41.91	352	210
S-3 [43]	577	477	3.20	1.21	149	10.50	101	41.91	317	210

[a]Note: The widths and thicknesses of the stiffeners (b_s and t_s) were not fully available in the literature. Stiffeners in the FE models were therefore designed per AASHTO, 2017 by the authors, and the t_s of all stiffeners used in the study is 12.7 mm (0.5 in.) to meet the AASHTO design requirement [3].

[b]Note: Sets {G7-T1, G7-T2} and {G8-T2, G8-T3} test two panels in the same girder to failure. When the panel in G7-T1 and G8-T2 failed, additional transverse or diagonal stiffeners were welded to the damaged panel to allow for subsequent testing of the next panel (G7-T2 and G8-T3).

Table 2
Comparison of FE and experimental shear capacity for selected boundary conditions.

Specimen	Experiment (Exp)	Finite Element (FE)											
		AR-NF		AF-NF		AR-WF		AF-WF		AF-WF-PE [PE = $D/10$]		AF-WF-PE [PE = $D/2$]	
	$V_{u.Exp}$ (kN)	$V_{u.FE}$ (kN)	$V_{u.FE}/V_{u.Exp}$	$V_{u.FE}$ (kN)	$V_{u.FE}/V_{u.Exp}$	$V_{u.FE}$ (kN)	$V_{u.FE}/V_{u.Exp}$	$V_{u.FE}$ (kN)	$V_{u.FE}/V_{u.Exp}$	$V_{u.FE}$ (kN)	$V_{u.FE}/V_{u.Exp}$	$V_{u.\ FE}$ (kN)	$V_{u.FE}/V_{u.Exp}$
G6-T1 [9]	516	518	1.00	298	0.58	552	1.07	384	0.74	445	0.86	475	0.92
G7-T1 [9]	623	636	1.02	361	0.58	654	1.05	440	0.71	522	0.84	579	0.93
G7-T2 [9]	645	636	0.99	361	0.56	654	1.01	440	0.68	522	0.81	579	0.90
G8-T1 [9]	375	413	1.10	265	0.71	469	1.25	397	1.06	439	1.17	443	1.18
G8-T2 [9]	445	567	1.27	328	0.74	606	1.36	421	0.95	488	1.10	518	1.16
G8-T3 [9]	516	567	1.10	328	0.64	606	1.17	421	0.82	488	0.95	518	1.00
2.2 [38]	75	73	0.98	43	0.57	87	1.16	62	0.82	69	0.92	74	0.99
US3/5 [39]	99	98	0.99	78	0.79	110	1.11	106	1.07	108	1.10	109	1.10
STG1 [40]	60	52	0.87	45	0.74	59	0.98	59	0.98	62	1.03	62	1.04
STG4 [40]	35	26	0.74	17	0.50	29	0.82	24	0.67	27	0.77	28	0.79
RTG1 [40]	40	41	1.02	23	0.59	42	1.06	28	0.69	34	0.86	38	0.95
RTG2 [40]	41	41	1.00	23	0.57	42	1.03	28	0.68	34	0.84	38	0.92
MSO [41]	94	98	1.04	52	0.55	103	1.10	67	0.71	80	0.85	91	0.97
CP1/1 [42]	88	87	0.99	52	0.59	97	1.10	67	0.76	77	0.88	81	0.92
S-2 [43]	161	155	0.96	140	0.87	181	1.12	174	1.08	180	1.12	181	1.12
S-3 [43]	198	208	1.05	148	0.75	213	1.07	184	0.93	206	1.04	206	1.04
Mean (μ)			1.008		0.643		1.092		0.837		0.944		0.997
Std. dev. (σ)			0.111		0.108		0.117		0.151		0.128		0.105

follow is based on a prototype girder adapted from the FHWA 2012 design example for a three-span continuous steel I-girder bridge [44], which has a web slenderness ratio of $D/t_w = 138$ as shown in Fig. 3. This prototype is proportioned to be representative of a common web slenderness ratio and has a depth that is larger than those listed in Table 1.

For simplicity, the following adaptations are made to the FHWA example design:

- the top flange is made identical to the bottom flange for symmetry,
- the stiffener spacing is parametrically varied to determine its effects on stress distribution, and
- the material strength of the flanges is chosen to be the same as the webs and stiffeners.

For all girder components of the prototype, the steel yield stress F_y was idealized as 345 MPa (50 ksi), the modulus of elasticity was 200 GPa (29,000 ksi), and the Poisson's ratio was 0.3. The dimensions of the prototype and mesh used in the corresponding FE model are shown in Fig. 3. Panel extensions of length $D/2$ are used in the PE models since Table 2 showed best correlation to experimental results. The other boundary conditions as represented in Fig. 1 will also be used to isolate the contribution of each girder component to the overall plate girder behavior. Panel lengths are represented by the variable a, which in these models equals the width of the panel in models that do not have explicit stiffeners, or the distance between the centerline of stiffeners for the S and PE models.

The FHWA 2012 prototype girder was modeled using the axially free boundary conditions described by Fig. 1; an aspect ratio (a/D) equal to one will be studied first. The strength results of the prototype study are presented in Table 3, where the prefix "1" is added to the nomenclature to indicate the a/D ratio. In Table 3, the results of the study are normalized by the simplest model with no flanges 1-AF-NF, to demonstrate the change that comes with explicitly modeling each girder component. It is seen that explicitly modeling the flanges (1-AF-WF) produces the greatest increase in elastic shear buckling load V_{cr} over the no flange model (1-AF-NF), where the flanges are represented by simple supports. In this case V_{cr} is increased by 31% since flanges offer increased fixity at the top and bottom web boundaries as noted by [11]. Progressively adding on stiffeners (1-AF-WF-S) and panel extensions (1-AF-WF-PE) raises V_{cr} by an additional 6% or 15%, respectively; these additions to V_{cr} can be explained by the rotational

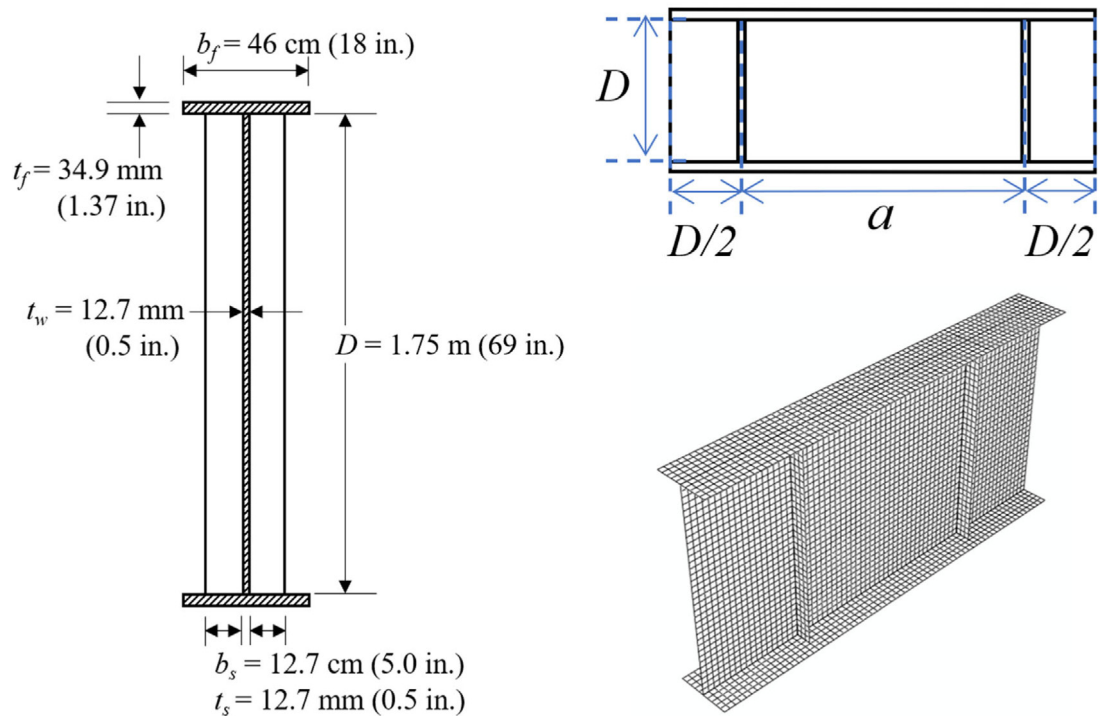

Fig. 3. Prototype dimensions, variable definitions, and mesh for the panel extension model. a/D ratios of 1, 2, and 3 will be studied.

restraint provided by the stiffeners and panel extensions instead of the free-rotation at the vertical web edges.

Similarly, the explicit modeling of flanges (1-AF-WF) produces an 18% increase in V_u over the simply supported model (1-AF-NF). The postbuckling shear reserve (defined by $V_u - V_{cr}$ [18]) represents the additional shear strength that is attained after elastic buckling. This postbuckling reserve is 426 kips for the 1-AF-WF model compared to the 584 kips for the 1-AF-NF model, showing a slight decrease when explicit flanges are modeled. Yet the increase in V_{cr} from the flanges is greater than the decrease in postbuckling reserve $V_u - V_{cr}$, resulting in an 18% higher V_u for the 1-AF-WF model. V_u continues to rise when stiffeners and panel extensions are explicitly modeled (in models 1-AF-WF-S and 1-AF-WF-PE, respectively), which assists in raising the postbuckling reserve $V_u - V_{cr}$ by 8% and 21%, respectively, over that of the flanges-only 1-AF-WF model. The substantial increase in the postbuckling shear reserve and V_u by the 1-AF-WF-PE model shows that the panel extensions play a large role in increasing the postbuckling reserve.

Model AR-NF is included in Table 3 to compare the different components of the ultimate postbuckling shear load (V_u) and postbuckling shear reserve ($V_u - V_{cr}$). Although V_u is similar between the AR-NF and the panel extension model, the AR-NF model has a much smaller elastic buckling value and a much larger postbuckling reserve value than the panel extension model. This result implies a different mechanism and load path, as will be shown later. Table 2 indicates that the AR-NF model correlates as well to the experimental data as does the panel extension model. It will be shown in Section 4.1 that the AR-NF model does not, however, capture the proper load path (and a proper model should capture both strength and load path).

3.4. Influence of imperfections

As previously noted, the experimental comparison FE models utilized an initial imperfection of $D/1000$. To examine the effects of initial imperfections, the imperfection magnitude is varied between $D/10{,}000$, $D/1000$ and $D/100$ [18,32,45]. A value of $D/10{,}000$ represents a negligible imperfection, with only minimal out-of-flatness provided to allow the buckling bifurcation to numerically occur [18]. $D/1000$ represents a small initial imperfection on the order of those recorded in girders in a typical steel fabrication shop [37]. $D/100$ represents the maximum allowable tolerance of initial imperfections in the industry, which is specified in detail by the AASHTO/AWS Bridge Welding Code [46].

The load–displacement curves are shown in Fig. 4 for the three different imperfection magnitudes on the AF-WF-PE model with a/D = 1.0 (shear loads V_{cr} and V_u are marked for each curve). The curves for $D/10{,}000$ and $D/1000$ imperfections are quite similar, while the $D/100$ curve displays a smaller shear stiffness and a slightly reduced V_u value (by 7%).

The point at which yielding occurs in the flanges are also marked. The first yield in the flanges occurs at the top left and bottom right corners of the girder panel, respectively (i.e., locations 1 and 2 in the inset figure of Fig. 4). This yielding occurs on the inside surfaces of the flange, 15 mm of vertical displacement beyond when the load–displacement curve reaches its ultimate postbuckling shear load V_u. Two other flange locations (3 and 4 in the inset figure of Fig. 4) yield after an additional 10 mm of vertical displacement along the unloading plateau. Both surfaces of the flange are observed to be at yield at all four locations after another subsequent 20 mm of vertical displacement. The four yield locations are similar to that theorized by Porter et al. [15], Fujii [14], the Cardiff model used in the Eurocode [35] and Reis et al. [47]. However, it is interesting to note that yield and hinging in the flanges occur significantly later in the unloading plateau, not at V_u (the max shear load); rather, V_u occurs when the web reaches high stresses and flange stresses are still relatively low (around 20 MPa).

Fig. 5 shows longitudinal stresses in the top flange above the top left corner of the web panel (location 1 in the inset figure of Fig. 4), where the tension field would be assumed to anchor in models used in the Eurocode [35]. The flange stresses at top, bottom and mid-surface are shown. The rate of change in the flange stresses shows no inflection at V_{cr}, similar to an experimental observation by [48]. Flange stresses are observed to increase appreciably only after reaching V_u (i.e., the rightmost load in Fig. 5) during the unloading plateau. This suggests that the flanges may be engaged in a secondary (post-ultimate load) load path after the web yields significantly in post-ultimate buckling, as suggested by [28].

Table 3
Shear strength results of models with different boundary conditions (a/D = 1.0 and D/1000 imperfection).

	V_{cr} (kN)	Normalized by 1-AF-NF	V_u (kN)	Normalized by 1-AF-NF	$V_u - V_{cr}$ (kN)	Normalized by 1-AF-NF
1-AF-NF	1982	1.00	2566	1.00	584	1.00
1-AF-WF	2596	1.31	3021	1.18	426	0.73
1-AF-WF-S	2714	1.37	3189	1.24	475	0.81
1-AF-WF-PE [PE = D/2]	2895	1.46	3442	1.34	547	0.94
1-AR-NF	1983	1.00	3583	1.40	1600	2.74

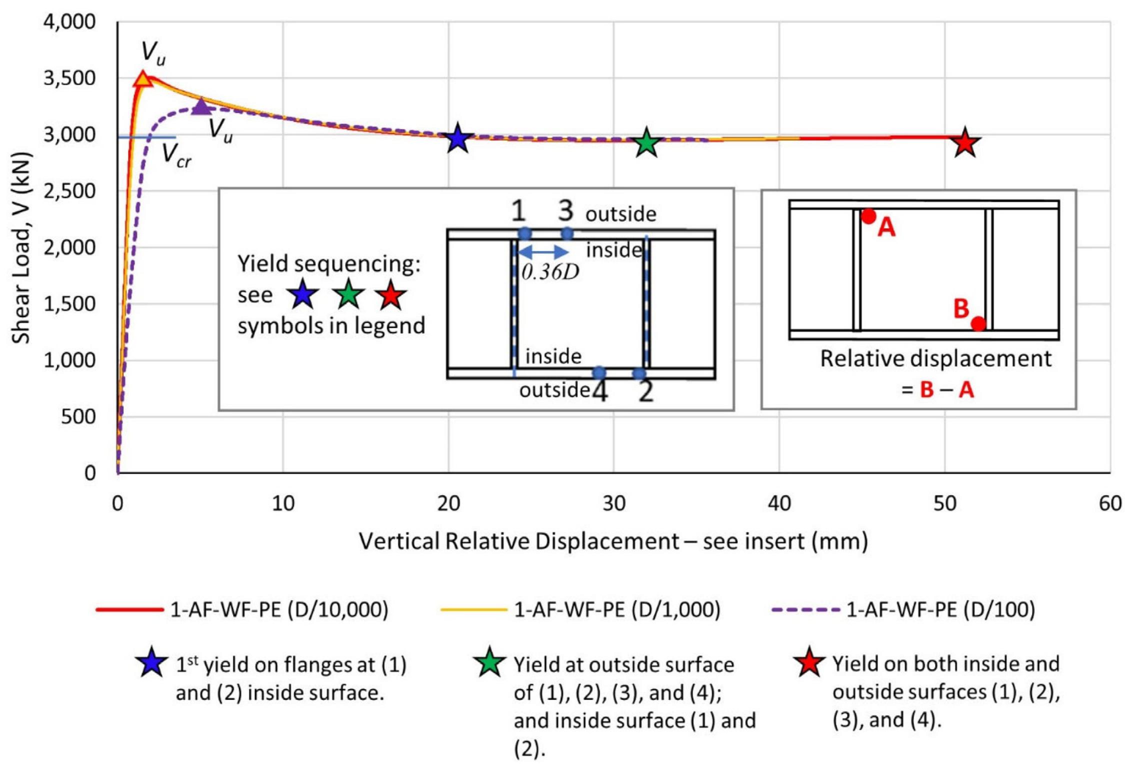

Fig. 4. Load vs. vertical displacement for imperfection iterations of the 1-AF-WF-PE model.

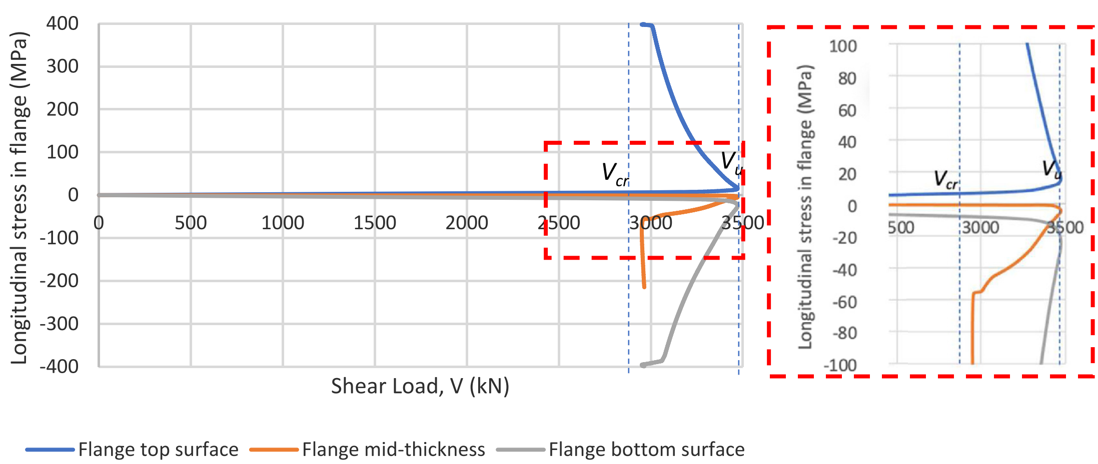

Fig. 5. Longitudinal stresses (*z*-direction, see Fig. 1) in the top flange above the top left corner of the web plate in the center panel (red dashed box is magnified).

The three imperfection magnitudes were also studied for the corresponding model without panel extensions (1-AF-WF-S), to determine if panel extensions affect how sensitive a model's shear strength is to imperfection magnitude. Table 4 displays the shear strength results for the three different imperfection values for models with and without panel extensions. Table 4 shows that the $D/10{,}000$ imperfection yields similar V_u results to the $D/1000$ imperfection for both models with and without panel extensions. Moving from a small imperfection ($D/1000$) to the maximum tolerable imperfection ($D/100$), a 13% reduction in V_u is observed for a model without panel extensions (1-AF-WF-S), in

Table 4
Imperfection sensitivity of the panel extensions boundary condition cases.

	V_{cr} (kN)	V_u (kN)	$V_u - V_{cr}$ (kN)	V_u normalized[a]
1-AF-WF-S ($D/10,000$)	2714	3202	487	1.00
1-AF-WF-S ($D/1000$)	2714	3189	475	0.996
1-AF-WF-S ($D/100$)	2714	2799	84	0.87
1-AF-WF-PE ($D/10,000$)[b]	2895	3479	584	1.00
1-AF-WF-PE ($D/1000$)[b]	2895	3442	547	0.99
1-AF-WF-PE ($D/100$)[b]	2895	3227	332	0.93

[a]Normalized by relevant $D/10,000$ model.
[b]Panel extensions [PE = $D/2$].

comparison to a reduction in V_u of only 7% for the model with panel extensions (1-AF-WF-PE). Importantly, the panel extensions reduce the imperfection sensitivity.

4. Load path analysis

4.1. Load path at the web plate edges

A major consideration for evaluating the load path in a buckled web is the determination of the forces at the web plate edges after buckling. The boundary conditions represent these web edges and thus validate the need for an extensive boundary condition study. In particular, the question to be answered is do the flanges and stiffeners anchor or carry some of the loads on the web plate edges, where the web intersects the flanges and stiffeners? Previous studies by Yoo and Lee [18], who studied a square plate that is simply supported on all 4 edges (i.e., without explicitly modeling the flanges and stiffeners), found that a web plate could develop substantial postbuckling shear capacity without the existence of normal stresses at the web edges; the web plate could self-equilibrate after buckling as long as an out-of-plane restraint existed at the web panel edges. This result suggests that the flange and stiffener may not play a role in the load path of the web plate.

This section replicates the boundary condition by Yoo and Lee (AF-NF) but for the prototype section of Fig. 3. Other boundary conditions such as that adding on flanges (AF-WF), stiffeners (AF-WF-S), and panel extensions (AF-WF-PE) are also studied. The objective is to observe whether changes in postbuckling behavior occur between models that explicitly include the flanges, stiffeners and adjacent panels versus those that include only 'virtual' flanges and stiffeners (which restrict out-of-plane translation via edge restraints, as done by Yoo and Lee [18]).

Fig. 6 illustrates the out-of-plane deformations of model 1-AF-WF-PE at V_u; a diagonal buckle is observed to form in the web panel, reaching 1.8 cm of lateral displacement. The buckled shapes for the other boundary condition models are similar. Fig. 7 plots the horizontal and vertical normal membrane stresses for all elements in the web for models 1-AF-NF, 1-AF-WF, and 1-AF-WF-PE at their respective ultimate postbuckling shear loads, V_u (given in Table 3). The "1" in front of the specified boundary condition indicates the model prototype (FHWA 2012 design example) and the web panel aspect ratio $a/D = 1.0$. It is seen that the stress distributions are related to the buckled shape of Fig. 6. In a state of pure shear before elastic buckling, membrane stresses normal to the element faces (hereafter called "normal stresses") are zero since the edges of the finite elements are parallel to or perpendicular to the pure shear loading (see Fig. 1). However, the onset of buckling induces normal stresses in the web plate elements.

Both horizontal and vertical normal stresses reach their most positive values (tension) in the center of the plate for all three models in Fig. 7 (1-AF-NF, 1-AF-WF and 1-AF-WF-PE); yet these positive normal stresses diminish moving from the plate center towards the web plate edges. In contrast, horizontal normal stresses are the most negative (compression) near the horizontal web edges associated with the flange, and vertical normal stresses are the most negative near the vertical web edges associated with the stiffener. For model 1-AF-NF with out-of-plane restraints at the web plate edges, the membrane stresses parallel to all four plate edges reach an order of about one-third of the yield stress (−118 MPa) in compression. However, the magnitude of these negative normal stresses reduces significantly if explicit girder components are modeled; when flanges are modeled in models 1-AF-WF and 1-AF-WF-PE, the horizontal stress at the web-to-flange edge drops to −22 MPa. Similarly, when stiffeners and panel extensions are modeled in 1-AF-WF-PE, the vertical stresses at the stiffener edges (AC and BD) are at largest −15 MPa. This result shows that full out-of-plane restraint at the web panel boundaries can lead to higher compressive stresses than when explicit girder components are modeled to restrain the boundary. The compressive stresses parallel to the web edges are on the order of 10% of yield when explicit girder components are modeled.

To assess whether the flanges, stiffeners, and panel extensions anchor any forces at V_u, Fig. 8 focuses on the membrane stresses normal to the web plate edges by studying models without flanges (1-AF-NF, 1-AR-NF), with flanges (1-AF-WF), with stiffeners (1-AF-WF-S), and with panel extensions (1-AF-WF-PE [PE = $D/2$]). Note that the results are symmetric due to the symmetric loading and boundary conditions (see Fig. 1), so the results at web plate edge AB are equivalent to those at DC, the results at web plate edge AC are equivalent to those at DB, etc. The purple dashed lines in Fig. 8 show the maximum and minimum normal stresses across all the elements in the web panel of model 1-AF-WF-PE (as shown in Fig. 7). It is seen that the maximum and minimum stresses from the whole plate are generally much larger than those normal to the edges.

The top and bottom web edges are examined in Fig. 8(b). When out-of-plane restraints are modeled at the web plate edges (model 1-AF-NF), the vertical membrane stresses normal to the top and bottom web edges are essentially zero at V_u (spikes in stresses only appear at the nodes directly on the web corners where the shear load is applied). When explicit flanges are modeled (1-AF-WF), there is no substantial change in the vertical membrane stresses at the top and bottom web edges; the vertical stresses are still essentially zero. This finding holds for all models with explicitly modeled flanges (including 1-AF-WF-PE, where the vertical stress on these edges does not exceed 5 MPa). This suggests that flanges do not anchor substantial membrane stresses at V_u and thus do not play a role in the postbuckling shear load path up to the ultimate postbuckling shear load V_u. The negligible vertical membrane stresses on the web-to-flange interface corresponds to the previous finding that the flanges have not yet yielded when the plate girder panel first unloads at V_u, instead reaching only 22 MPa (i.e., less than one-tenth of yield stress). High flange stresses and plastic hinges are observed to form much later along the unloading plateau (as noted previously in Fig. 4).

Fig. 8(a) examines the left and right edges of the web panel at V_u. The membrane stresses normal to these edges are essentially zero for the 1-AF-NF, 1-AF-WF, and 1-AF-WF-S models. In comparison to an out-of-plane restraint, the presence of the explicitly modeled stiffener in 1-AF-WF-S does not change the horizontal stress, suggesting that the stiffener does not anchor horizontal membrane stresses up to V_u. However, horizontal membrane stresses exist when the panel extensions are added beyond the stiffener. It is also important to note the large magnitude of stresses for the 1-AR-NF model, which is restrained along its longitudinal axis on the vertical edges. These stresses are an order of magnitude larger than those for the 1-AF-WF-PE model. Both models show good agreement with the experimental strength results, yet the 1-AR-NF model does not capture the proper flow of stresses within the plate — its boundary condition is artificially rigid and thus attracts too much force near the vertical edges of the web. Hence, going forward, only the panel extension (PE) model with $D/2$ extension as illustrated in Fig. 3 will be used for studying membrane stresses.

In the PE cases, stresses flow past the stiffener and continue into the adjacent web panel (panel extension), as illustrated in Fig. 9. The horizontal membrane stresses are now non-zero at the vertical edges

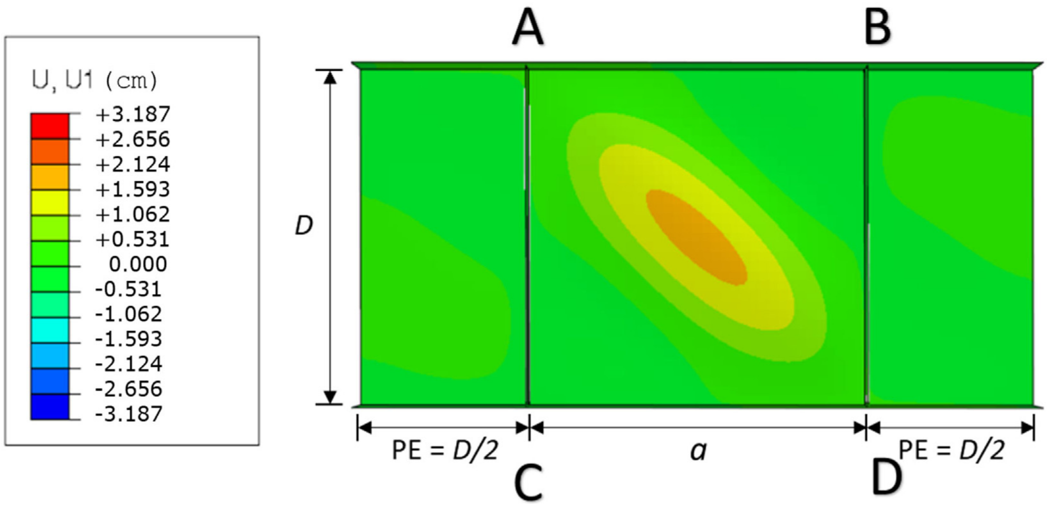

Fig. 6. Out-of-plane displacement at V_u in 1-AF-WF-PE Model for D/1000 imperfection. Units: centimeters. Positive displacement is out of the page. The maximum displacement is 1.8 cm at the center of the buckle. The contour scale matches the contours of Fig. 10 for comparative purposes.

of the plate (AC and BD), where the stresses reach a maximum of 20 MPa and thus still small in comparison to the 345 MPa yield stress. However, by integrating the horizontal membrane stresses along the vertical edge of the plate, a substantial 214 kN of horizontal tension force is observed to pull on the adjacent panel extension, which is equal to approximately 40% of the postbuckling shear reserve of the model. In addition, it was shown in Table 3 that not only is the ultimate postbuckling shear load V_u of model 1-AF-WF-PE larger than that with no panel extensions (1-AF-WF-S), but the postbuckling shear reserve ($V_u - V_{cr}$) also increases. This finding from the panel extension models matches well with previous research that the presence of an adjacent rigid/non-rigid end post influences postbuckling shear strength of end panels [16,49].

It is important to note that no substantial compression is observed in the explicitly modeled stiffener; by summing the axial force contribution across the width of each 2-sided stiffener, the stiffener axial force is observed to be less than 9% of the expected postbuckling shear reserve $V_u - V_{cr}$ for the 1-AF-WF-PE model. Vertical stiffeners are primarily loaded in bending by providing lateral restraint to the web, with only small levels of axial compression. The axial stress in the stiffener is less than 5% of yield, while bending stresses reach around 10% of yield.

The load path findings for web panels with $a/D = 1$ can be extended to the larger aspect ratios of $a/D = 2$ and 3 using model boundary condition AF-WF-PE. Larger panel aspect ratios are commonly used in industry, while $a/D = 3$ is the limit that distinguishes transversely stiffened and unstiffened girders in the AISC [4] and AASHTO [3] design codes. Fig. 10 shows the out-of-plane deformations at V_u of models with $a/D = 2$ (2-AF-WF-PE) and $a/D = 3$ (3-AF-WF-PE) and $D/1000$ imperfection. In contrast to the single buckle of the 1-AF-WF-PE model, two and three diagonal buckles are observed to form in the web panel of 2-AF-WF-PE and 3-AF-WF-PE, respectively, reaching maximum lateral displacements of 2.8 cm and 3.2 cm, respectively. The lateral displacements of these two models are 1.6 and 1.8 times larger, respectively, than that of the smaller aspect ratio model 1-AF-WF-PE.

Figs. 11 and 12 show the horizontal and vertical membrane stresses at V_u, respectively, for the 2-AF-WF-PE and 3-AF-WF-PE models. Similar findings as for the $a/D = 1$ plate are observed for these cases; near-zero normal stresses exist at the top and bottom of the web (AB and DC) thus indicating that the flanges do not vertically anchor substantial web stresses at V_u. On the left and right web edges (AC and DB), horizontal normal stresses reach magnitudes of about 24 MPa and 11 MPa in the $a/D = 2$ and $a/D = 3$ models, respectively, where in both cases these values are small compared to the maximum horizontal membrane stress at the center of the panel. As in $a/D = 1.0$, the stiffeners do not play a significant role in the load path in the plane of the web and instead mostly provide lateral restraint to the web. The maximum horizontal membrane stresses in the entire plate vary from 67 MPa, to 140 MPa, to 130 MPa for a/D values equal to 1.0, 2.0 and 3.0, respectively. The vertical membrane stresses consistently decrease as the aspect ratio increases.

4.2. Load path of principal membrane stresses

Principal membrane stresses indicate the direction and magnitude of the tension and compression stresses and thus are a useful tool for evaluating load paths. In a state of pure shear, the load paths of tension and compression occur on perpendicular diagonals offset 45 degrees from the horizontal. An element in pure shear is loaded in equal and opposite tension and compression. For the prototype of this study (Fig. 3) and the panel extensions boundary condition (Model 1-AF-WF-PE), the elastic buckling stress, $\tau_{cr} = \frac{V_{cr}}{Dt_w}$ equals 130 MPa, where V_{cr} is determined from the first eigenvalue FE analysis. The analyses presented in this section evaluate stresses in the web once the shear load exceeds V_{cr}. Such an examination tests the assumptions of tension field action (i.e., that compression stresses can be neglected) and also reveal the path of forces leading to the ultimate postbuckling shear load, V_u.

4.2.1. Contours of principal membrane stresses for a/D = 1.0

Fig. 13 plots the contours of principal membrane stresses at V_u for the web panel with $a/D = 1$. The coloring in this plot represents the following:

- The thick black line represents the elastic buckling stress, τ_{cr}.
- The orange shaded band inside of the bold black line represents stresses below τ_{cr}.
- The thick pink line represents the ultimate shear stress $\tau_u = V_u/(Dt_w) = 154.7$ MPa for the $a/D = 1$ model.
- The green shaded bands represent compressive membrane stresses that fall between τ_{cr} and τ_u.
- The pink shaded bands show where compressive stresses are at a magnitude greater than τ_u.

Fig. 13(a) shows that a large portion of the plate panel is shaded green or pink, indicating stresses above τ_{cr}. This runs contrary to conventional tension field theories, which assume that at the ultimate load, compressive stresses do not increase beyond τ_{cr}. Compressive stresses are concentrated in the outer (pink) bands of the plate where

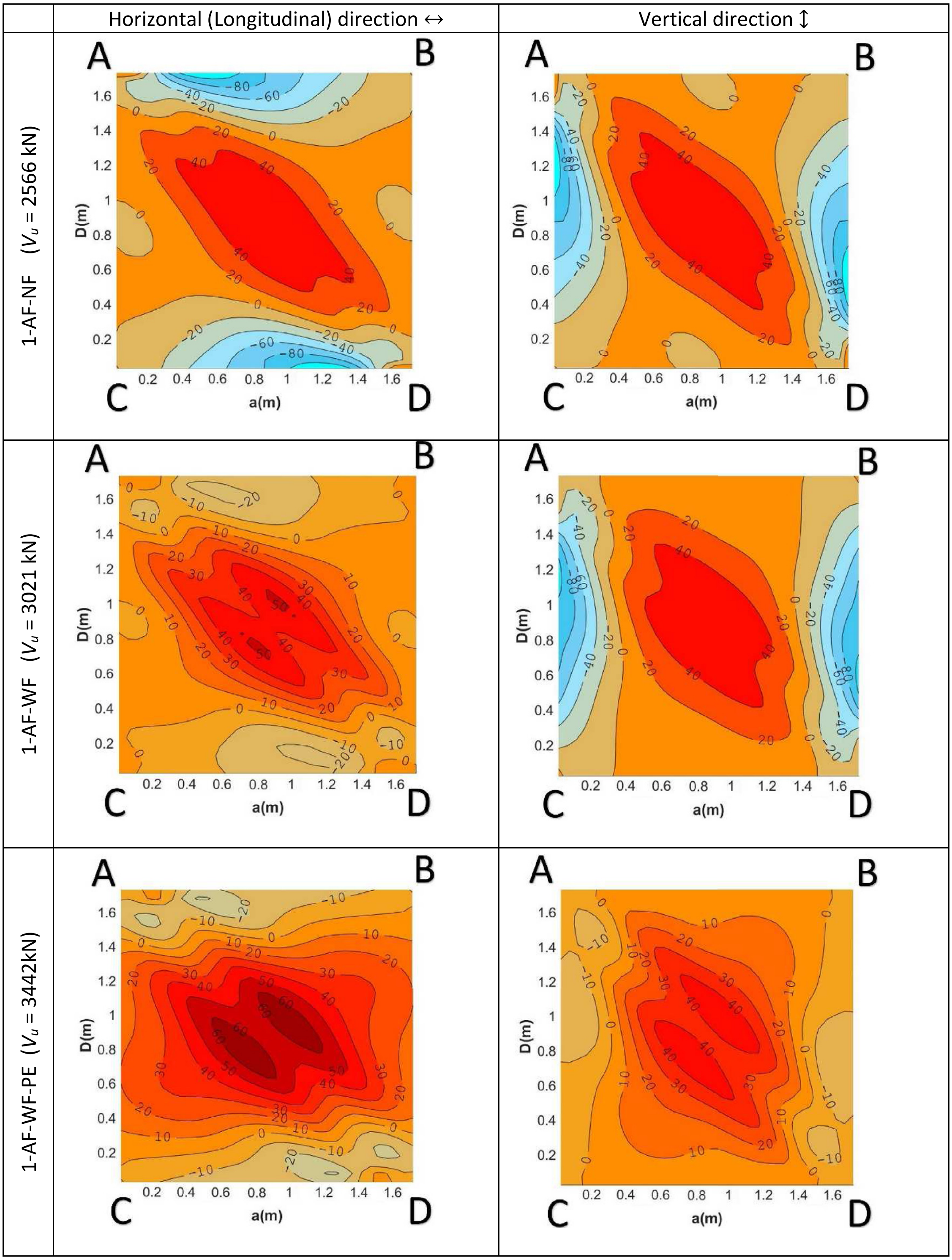

Fig. 7. Membrane stresses at V_u in the web plate panel for the 1-AF-NF, 1-AF-WF, and 1-AF-WF-PE models (contour units are in MPa).

compressive stresses increase between 19% and 50% above τ_{cr} , and up to 26% above τ_u. Fig. 13(b) demonstrates that the principal membrane tensile stresses increase essentially throughout the plate. The pink and green bands indicate that the tension field varies in magnitude, with a roughly bell-shaped distribution similar to that theorized by Steinhardt and Schroter [50]. The tensile membrane stresses in the pink band have increased between 19% to 67% above τ_{cr}.

In Mohr's circle, the maximum and minimum principal stresses are on opposing ends of the circle; their average is at the center of the circle. Fig. 13(c) shows the stress at the center of Mohr's circle for each element in the web plate. In a state of pure shear, Mohr's circle would be centered at zero stress. However, if the maximum (tensile) principal stress is greater than the minimum (compressive) principal stress, the circle would be centered on a positive value (red shaded region of Fig. 13(c)). Conversely, if the compressive principal stress is greater than the tensile principal stress, the circle would be centered on a negative value (blue shaded region of Fig. 13(c)). Therefore, the center of Mohr's circle indicates whether compressive stress or tensile stress predominates at a given location, as well as by how much. At the center of the plate, tension predominates as the center of Mohr's circle

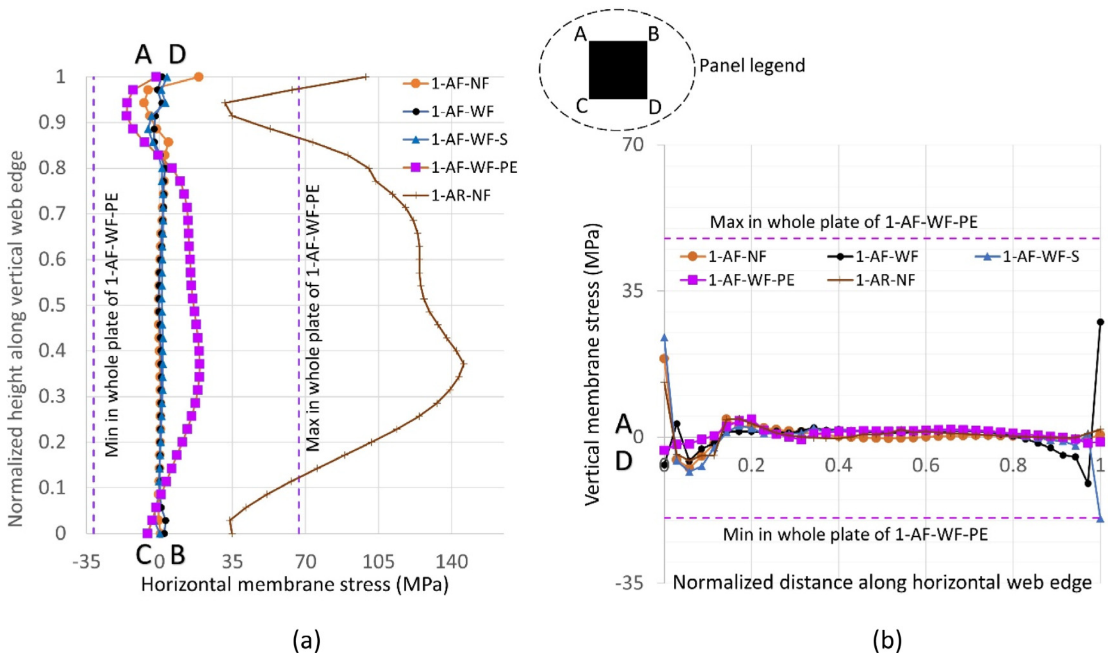

Fig. 8. Membrane stresses at V_u along the web panel edges for various boundary conditions: (a) Horizontal (↔) Membrane Stress Along Left (AC) and Right (DB) Edge of Web Panel. (b) Vertical (↕) Membrane Stress Along Top (AB) and Bottom (DC) Edge of Web Panel. See Panel legend for lettering scheme of edges. Distances are normalized by the web depth D = 1.7526 m.

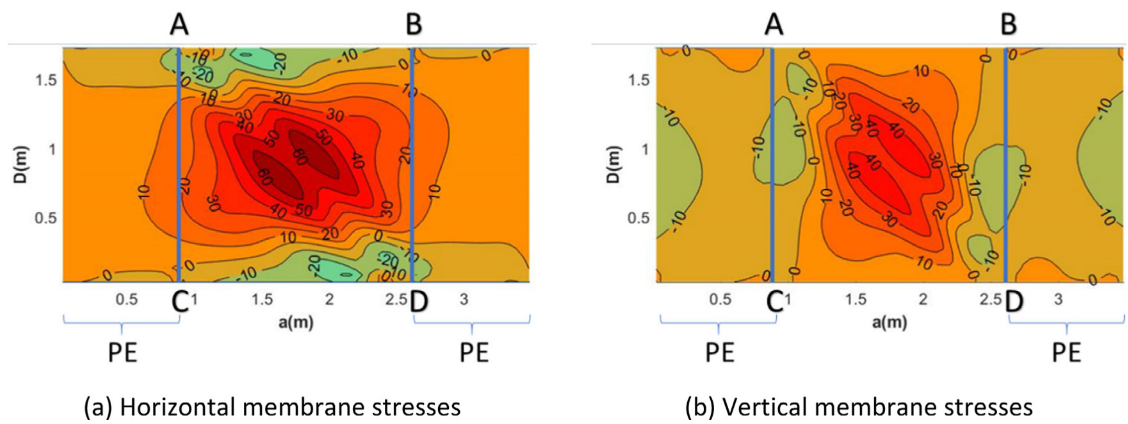

Fig. 9. (a) horizontal and (b) vertical membrane stresses at V_u in web panel and panel extensions (PE) in 1-AF-WF-PE model with PE = D/2 extensions. The vertical blue lines AC and BD represent the stiffeners that start the panel extensions on either side of the center panel. Units of contours = MPa. (For interpretation of the references to color in this figure legend, the reader is referred to the web version of this article.)

reaches +57.2 MPa, meaning that tensile stress exceeds compressive stress at the center of the plate by up to 114.4 MPa (in agreement with tension field theories). However, near the top and bottom edges of the plate, the center of Mohr's circle reverses sign and reaches −18.1 MPa, meaning that the compressive stress actually exceeds tensile stress by up to 36.2 MPa near the top left and bottom right corners of the plate. The portions of the plate in pure shear are located at the boundary between the blue and red shaded regions where the center of Mohr's circle is 0 MPa. However, all edges of the web plate are relatively close to a pure shear state, with the center of Mohr's circle varying no more than +6 MPa in the red regions on the edge and −12 MPa in the blue regions on the edge.

While the focus of this paper is to examine the flow of forces (and thus membrane stresses are more suitable per Section 2), it is also interesting to examine whether the plate has yielded via both the membrane stresses (which neglect bending) and the stresses on the plate surfaces (which consider bending). Fig. 13(d) shows the von Mises stresses calculated from the principal membrane stresses. The highest von Mises stresses occur at the corners of the plate at the ends of the tension field, where both maximum and minimum principal membrane stresses are observed to be large. These corners are also on either end of the diagonal buckle at V_u in Fig. 6. It is interesting to note that considering the membrane stresses only, the von Mises stresses reach a maximum of 330 MPa, approaching but still below the yield stress F_y = 345 MPa. However, examining the stress state on the two surfaces of the web plate, Fig. 14 indicates that von Mises yield stress is reached. This reflects the finding from Garlock et al. [20] that second-order bending stresses (i.e., through-thickness bending stresses that are not considered in the membrane stresses) are large contributors to reaching yield in the web plate. Fig. 14 shows that high stresses in the center panel tend to continue into the adjacent panel extensions, though they diminish in magnitude.

Fig. 15 shows the angles (θ_p) of the (a) minimum and (b) maximum principal membrane stresses in the plate. The angle of the minimum principal membrane stresses decreases from 45° at the top and bottom of the plate (becoming slightly more horizontal) and increases at the

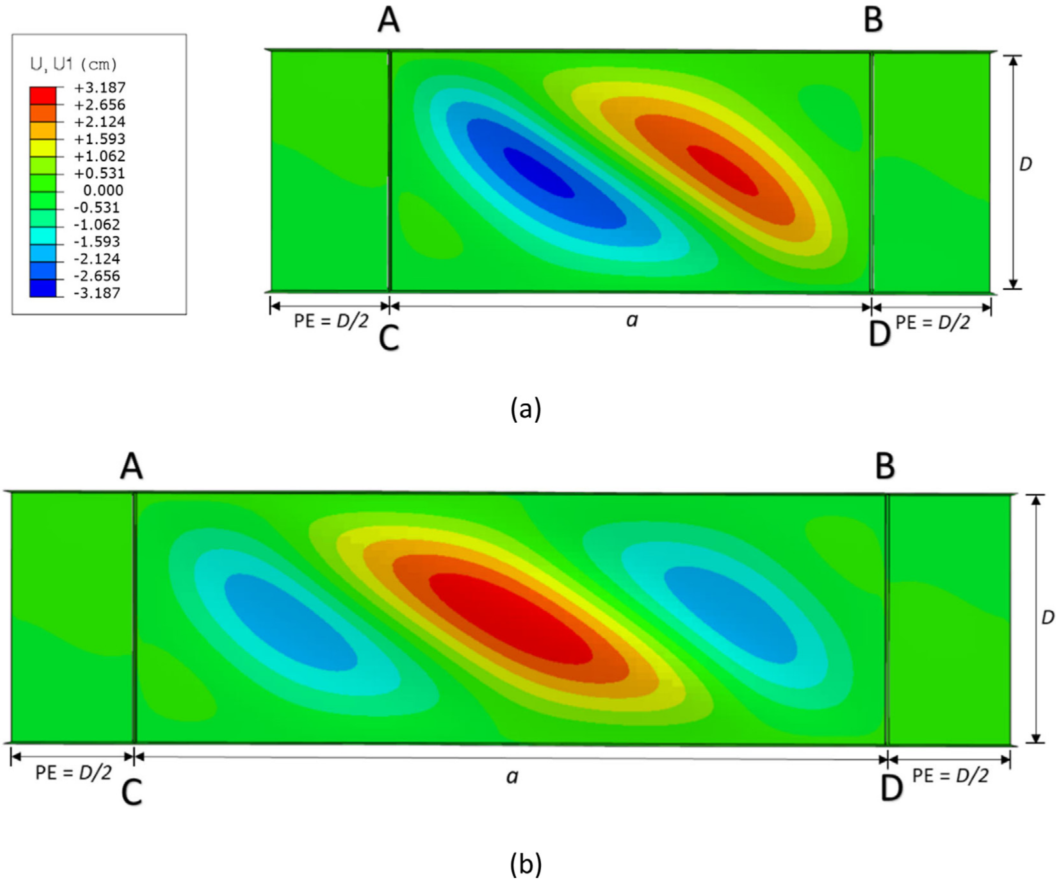

Fig. 10. Out-of-plane displacement at V_u for models: (a) 2-AF-WF-PE, (b) 3-AF-WF-PE for D/1000 imperfection. Positive displacement is out of the page. Units: centimeters.

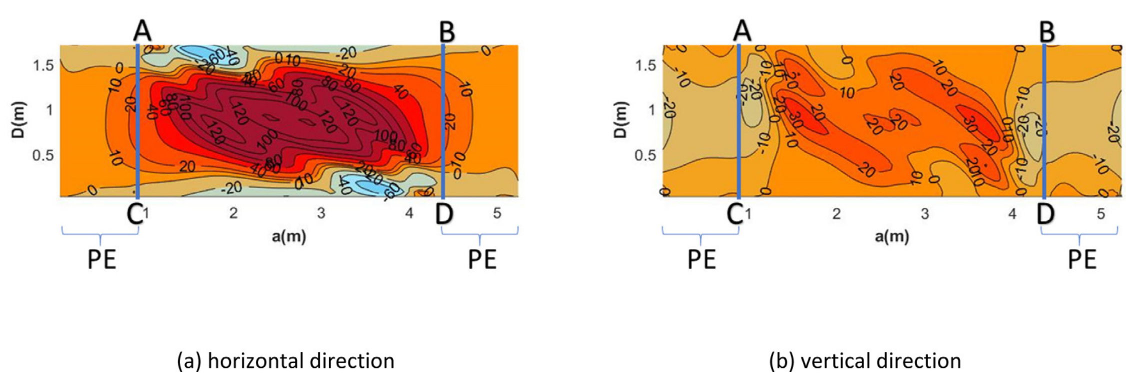

Fig. 11. Membrane stresses in the web plate for the 2-AF-WF-PE model: (a) horizontal (longitudinal) direction, and (b) vertical direction. Units of contours = MPa.

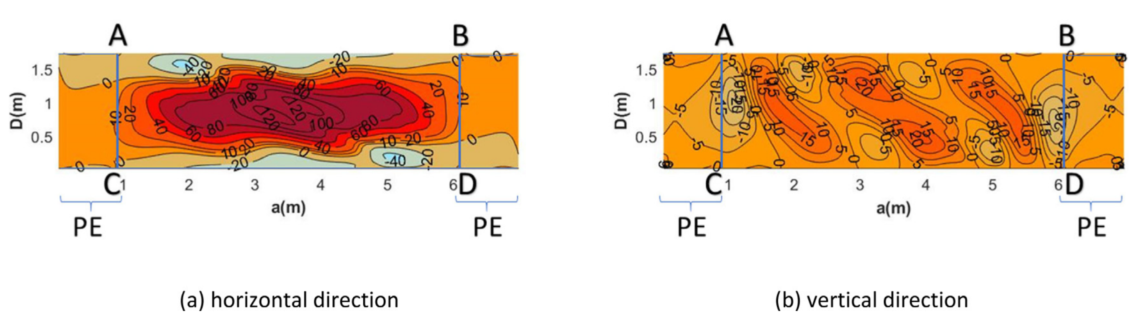

Fig. 12. Membrane stresses in the web plate for the 3-AF-WF-PE model: (a) horizontal (longitudinal) direction, and (b) vertical direction. Units of contours = MPa.

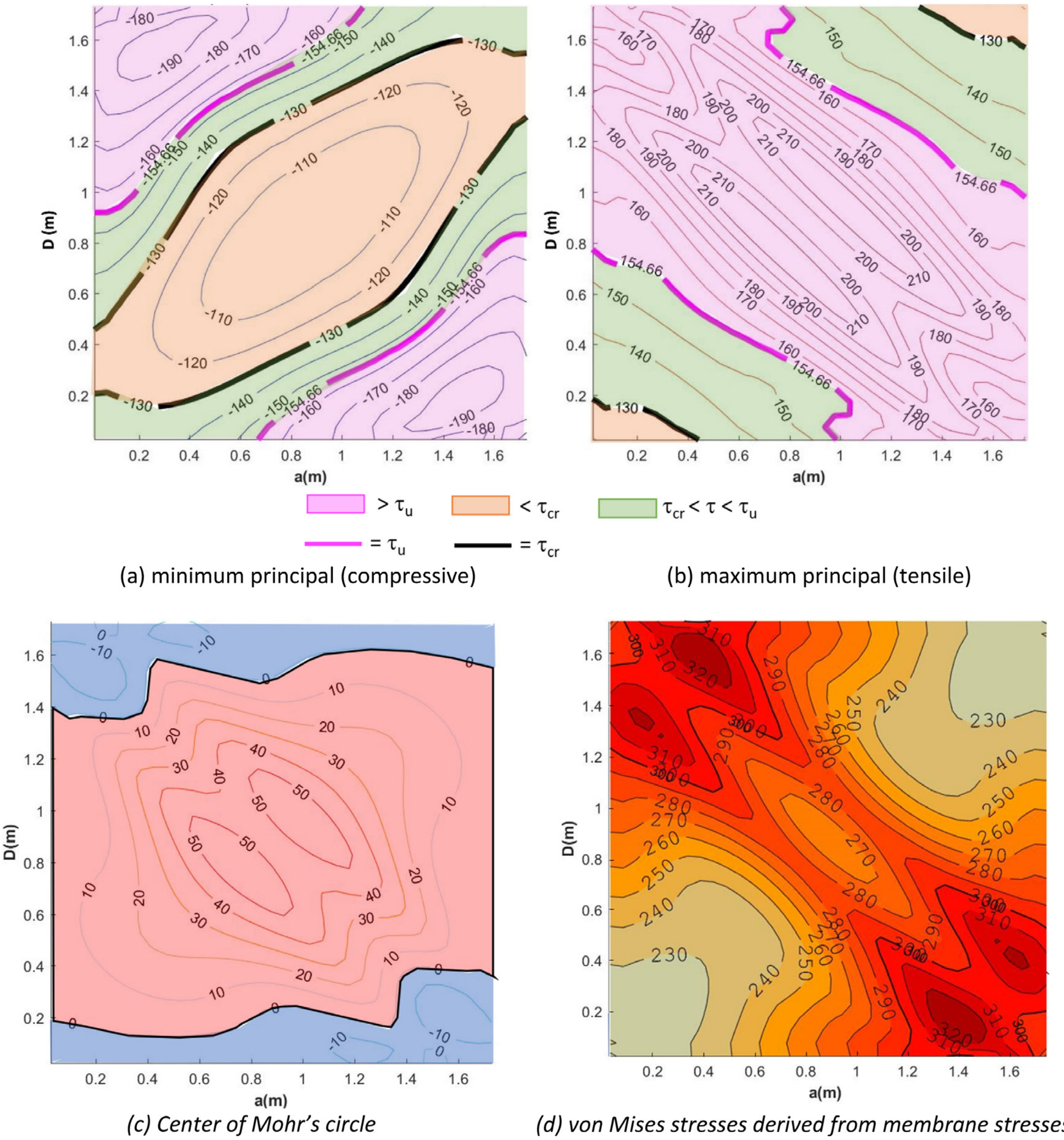

Fig. 13. Contour of principal membrane stresses at V_u of 1-AF-WF-PE (center panel), D/1000 imperfection. Units of contours = MPa. (For interpretation of the references to color, the reader is referred to the web version of this article.)

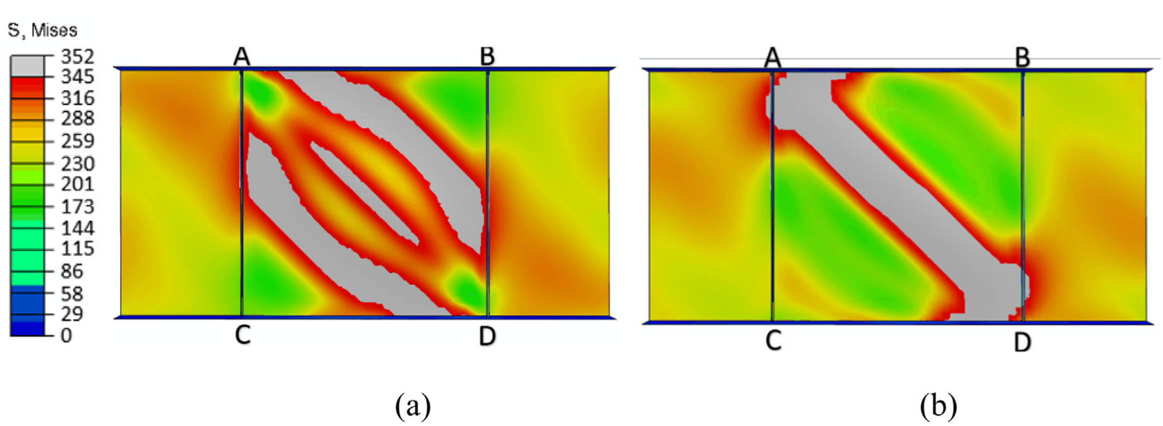

Fig. 14. von Mises stresses (units: MPa) on (a) front surface and (b) back surface of model 1-AF-WF-PE at V_u. Gray denotes regions of von Mises yield. (For interpretation of the references to color in this figure caption, the reader is referred to the web version of this article.)

vertical left and right edges of the plate (becoming slightly more vertical). However, the angles do not deviate from 45° by more than 4° at any location on the web panel.

4.2.2. Effects of initial imperfections for $a/D = 1.0$

While it was shown previously that an initial imperfection of $D/1000$ captures the V_u of typical plates and correlated well to experimental results, it is important to quantify the influence of initial imperfection magnitude on the response of the plate leading up to V_u (as already observed by a change of stiffness in Fig. 4). Where until now the results were only shown at V_u, this additional imperfection study provides insight to the plate behavior and the redirection of load path as the shear increases from zero to V_{cr} to V_u. This section evaluates the same three different initial imperfections as before: $D/10{,}000$, $D/1000$, and $D/100$.

As shown in Table 4, the ultimate postbuckling shear loads V_u are similar in all three cases (3479, 3442, and 3227 KN, respectively); however, Fig. 16 shows that the evolution of stresses varies with initial imperfection. The minimum (compressive) principal membrane stresses are shown for the elements that lie on the 'tension diagonal' defined by a line connecting points A and D as shown. Each curve represents a different element, where the colors are defined per Section 4.2.1 (and shown in Fig. 13(a)). Note that since the results are symmetric, it appears as though only half the elements on the diagonal are plotted. The elastic shear buckling load V_{cr}, the ultimate postbuckling shear load V_u, the elastic buckling shear stress τ_{cr}, and the ultimate shear stress τ_u are marked with dashed lines. The following is observed:

- For the $D/10{,}000$ model, a clear bifurcation is observed at V_{cr}, where the stresses leading up to V_{cr} are equal for all elements and then "fan-out" as the stresses redistribute after reaching V_{cr}. A clear buckling response is not observed at V_{cr} in the models with larger imperfections ($D/1000$ and $D/100$). The stresses in the D/1000 model fan-out at approximately two-thirds V_{cr}, and the D/100 model initiates its dispersion of compressive stresses at the onset of loading.
- The green and pink elements have compressive stresses greater than τ_{cr} (130 MPa) at V_u, indicating a departure in behavior from that predicted by conventional Tension Field Action theory and Rotated Stress Field theory as discussed previously [10,16]. These green and pink elements occur for all imperfection magnitudes.
- The blue line in each plot represents the initial slope of the plot, thus describing a linear membrane stress increment with increasing shear load (i.e., the idealized membrane stress in pure shear if the effects of buckling are not considered). After elastic buckling, the green elements continue to increase above τ_{cr} after elastic buckling but at a slower rate than before elastic buckling (these are above the blue line). The pink elements continue to increase after elastic buckling but at a rate greater than before elastic buckling (these are below the blue line). Compression forces are thus further engaged after buckling than before buckling in the pink regions of the plate. These compression loads have redistributed from the orange elements near the center of the plate and concentrated in these pink regions. The higher compressive stresses serve to equilibrate some of the tension stresses instead of having them anchor onto the flanges or stiffeners.

In summary, the compression forces redistribute after elastic buckling, concentrating in elements near corners A and D and unloading in the plate center where the buckled displacement is largest (see Fig. 6). While the magnitude of initial geometric imperfection influences when the buckling redistribution of stress occurs, similar compressive load redistribution is observed for all imperfections.

For comparison, the maximum (tensile) principal membrane stresses of the same elements are plotted vs. applied shear load in Fig. 17 for a $D/1000$ imperfection (since the imperfection findings are similar to those from Fig. 16, the other imperfections are not shown here for brevity). The tensile principal stresses increase in all elements and at an increased rate than before elastic buckling (i.e., above the blue line in this plot). Compared to the minimum (compressive) principal membrane stresses shown in Fig. 16(b), the magnitude of maximum tensile membrane stress is similar to the maximum magnitude of compressive stresses, although the average tensile stress is larger. Elements that unload in compression stress (orange) are shown to increase the most in tension stress, though this only occurs in the center of the plate.

Note that in Fig. 17 there is a discontinuity (or a "kink") in the stress load plot between V_{cr} and V_u at which the tensile stresses continue to increase, but at a smaller rate. Similarly, in Fig. 16(b), the increase of compression stress at this shear load value accelerates in the elements near the corners but attenuates at the center of the panel. As shown in Fig. 18, the changing rate of stresses corresponds to a significant decrease of stiffness in the shear load–displacement behavior. In summary, the load path changes and the membrane forces redistribute as the web panel loses stiffness, presumably due to significant yielding in the buckled web panel. The formation of this mechanism will be studied further by the authors in future publications.

4.2.3. Load path of principal membrane stresses for $a/D > 1.0$

V_{cr} decreases with increasing a/D, as expected, where the V_{cr} values are equal to 2894 kN, 2054 kN, and 1929 kN for a/D values of 1.0, 2.0, and 3.0, respectively. V_u similarly decreases with increasing a/D, where the V_u values are equal to 3442 kN, 2898 kN, and 2694 kN for a/D values of 1.0, 2.0, and 3.0, respectively. Fig. 19(a) and (b) plot the minimum and maximum principal membrane stresses at V_u for the $a/D = 2.0$ panel, and Fig. 19(c) and (d) plot the same for the $a/D = 3.0$ panel. The colors in these plots are coded in the same way as described in Section 4.2.1. It is seen that for all three a/D ratios, the same pattern develops in the principal stresses as discussed for $a/D = 1.0$. Though not shown here, the von Mises stresses calculated from membrane stresses at V_u are lower for $a/D = 2.0$ and 3.0 than for $a/D = 1.0$, reaching maximum values of 320 and 268 MPa (93% and 78% of yield, respectively), at the ends of the tension field. This highlights the larger role of second order bending stresses in causing yield at V_u in higher aspect ratio plates. Fig. 20 shows that when a/D increases, at the center of the plate, the angles of principal tensile stresses become more horizontal and the angles of principal compressive stresses become more vertical, deviating from 45° by greater than 10 degrees. The angles at the top and bottom of the plate deviate less than the plate center.

5. Conclusions

This paper presented a detailed examination of various boundary conditions on slender steel plates with pure shear loading conditions. The influence of modeling each girder component on the plate boundary (e.g., flanges, stiffeners, and adjacent web panels) and the effects of initial imperfections were assessed. The boundary condition models were compared with a suite of 16 experimental tests, representing a range of web depths (D), panel aspect ratios (a/D), and web slenderness ratios (D/t_w). The effects of the boundary conditions on the membrane stresses at the web plate edges and principal membrane stresses in the web were also examined for panel aspect ratios of 1, 2, and 3. The following conclusions can be made based on the results of this evaluation:

- Finite element (FE) models of a plate under pure shear should include flanges, stiffeners, and "panel extensions" as the boundary conditions (with axially free vertical edges at the ends of the web panel) if possible, for best correlation with experimental results. The panel extensions (which extend the girder web and flange for a distance $D/2$ beyond the stiffeners on each side of the web) produce the best agreement with the experimental literature and also best represent the membrane stresses at the plate edges for a continuous girder section.

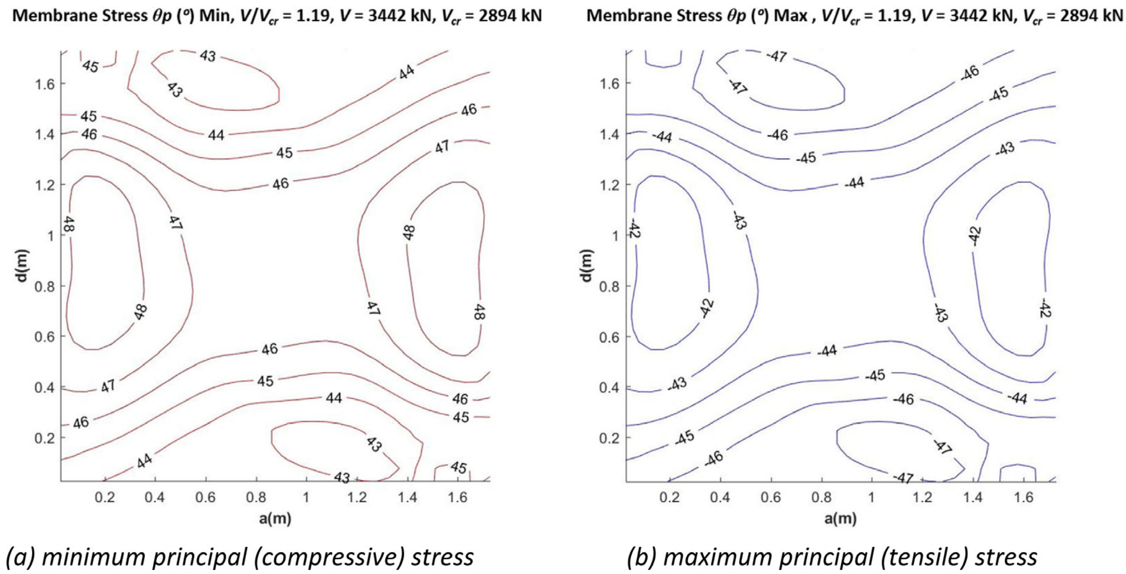

Fig. 15. Angles (θ_p) of principal membrane stresses at V_u for 1-AF-WF-PE, D/1000 imperfection. Units of contours = degrees. Positive and negative values signify counterclockwise and clockwise rotation from horizontal, respectively.

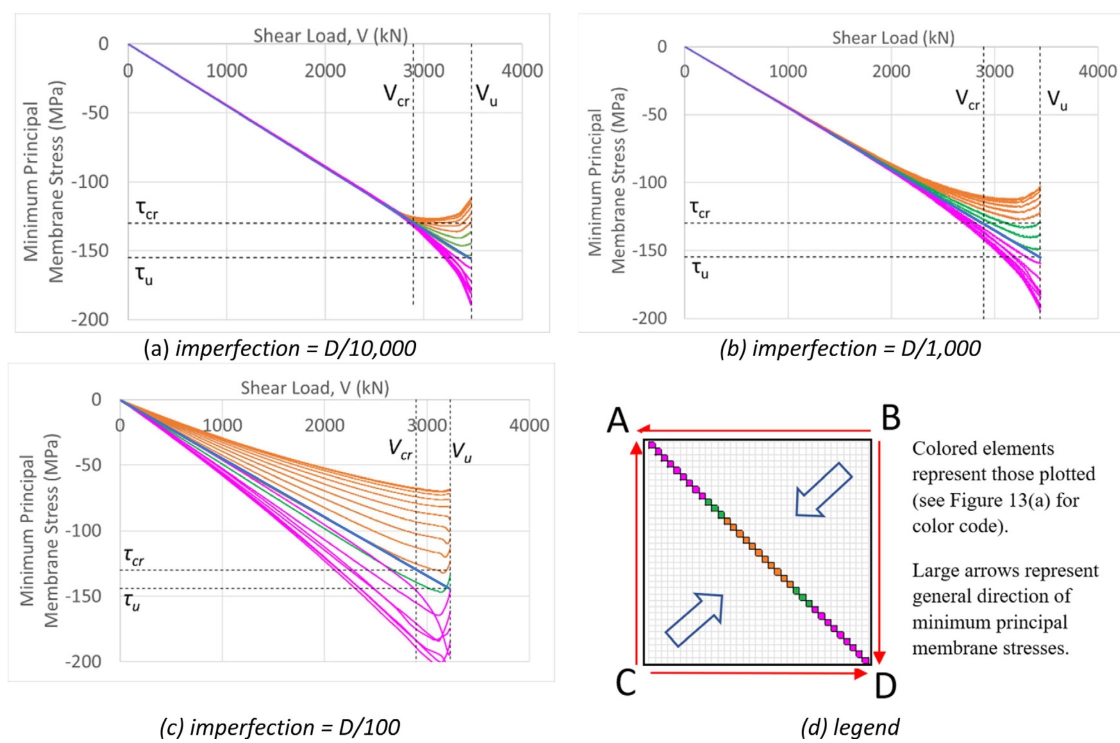

Fig. 16. Minimum (compressive) principal membrane stresses in elements along the web diagonal vs. applied shear load for model 1-AF-WF-PE, for three different imperfection magnitudes. The blue line on Fig. 16(a), (b), and (c) represents the continuous slope of the elastic regime extended up to V_u. (For interpretation of the references to color in this figure caption, the reader is referred to the web version of this article.)

- Panel extensions longer than $D/2$ were not observed to appreciably increase the elastic shear buckling load V_{cr} or the ultimate postbuckling shear load V_u.
- Modeling the flanges enables a non-negligible increase in elastic shear buckling load V_{cr} due to the large degree of rotational restraint that it adds to the top and bottom edges of the web versus a simply restrained boundary condition.
- The horizontal membrane forces at the left and right (i.e., vertical) edges of each web panel play a role in determining how much postbuckling shear strength can be achieved. For this reason, axially restrained boundary conditions at these vertical edges can overestimate the horizontal forces. Including panel extensions (or heavier end-post stiffeners) can better capture the flow of forces beyond the buckled panel, representing the continuity of the plates in a girder assembly without the need to model the full girder.
- The membrane stresses normal to the vertical edge, where the stiffener is located, are essentially zero if a panel extension is not modeled. Adding a panel extension results in normal membrane stresses on this vertical edge that reach about 10% of the yield stress at V_u.

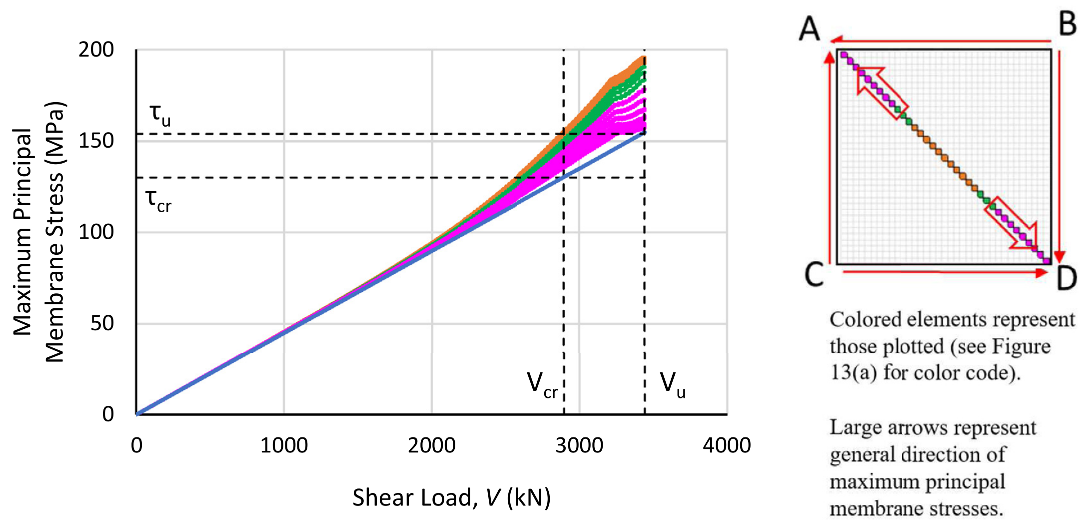

Fig. 17. Maximum (tensile) principal membrane stresses vs. shear load applied for model 1-AF-WF-PE and D/1000 imperfection. The blue line represents the continuous slope of the elastic regime up to V_u. (For interpretation of the references to color in this figure caption, the reader is referred to the web version of this article.)

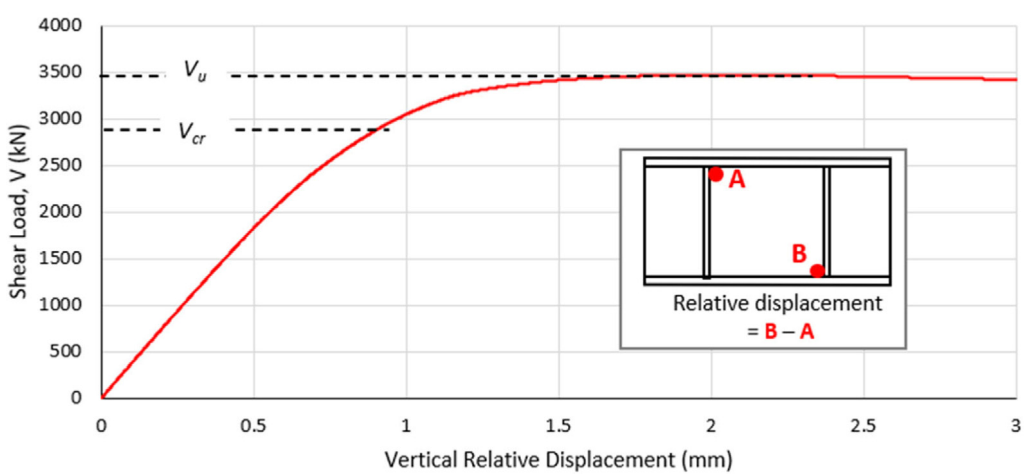

Fig. 18. Shear load versus vertical relative displacement for model 1-AF-WF-PE and D/1000 imperfection.

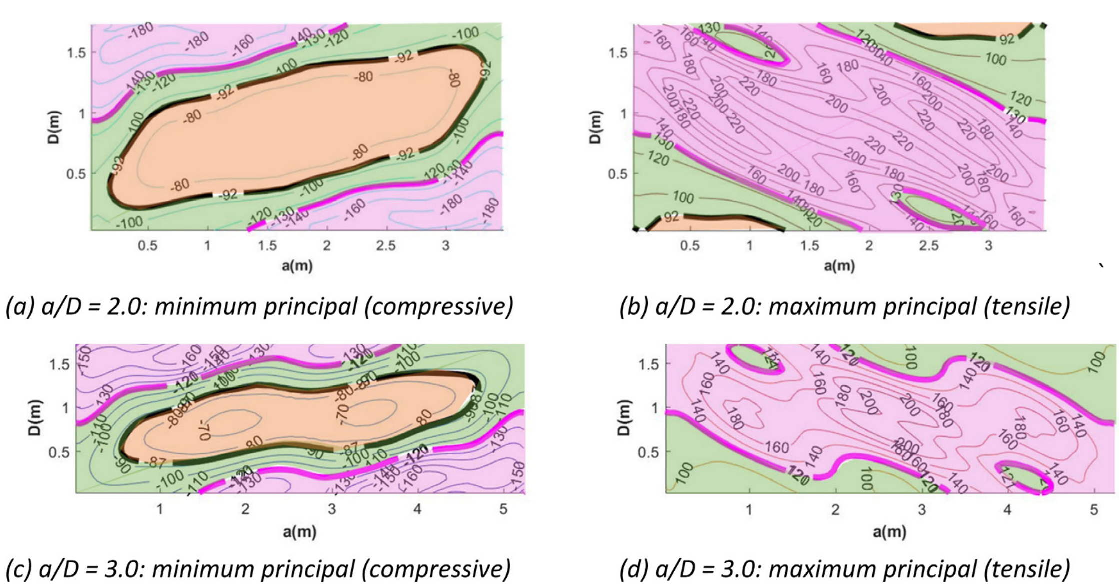

Fig. 19. Contour of principal membrane stresses at V_u for AF-WF-PE models (center panel) with D/1000 imperfection for (a–b) $a/D = 2.0$ and (c–d) $a/D = 3.0$. Units of contours = MPa. (For interpretation of the references to color, the reader is referred to the web version of this article.)

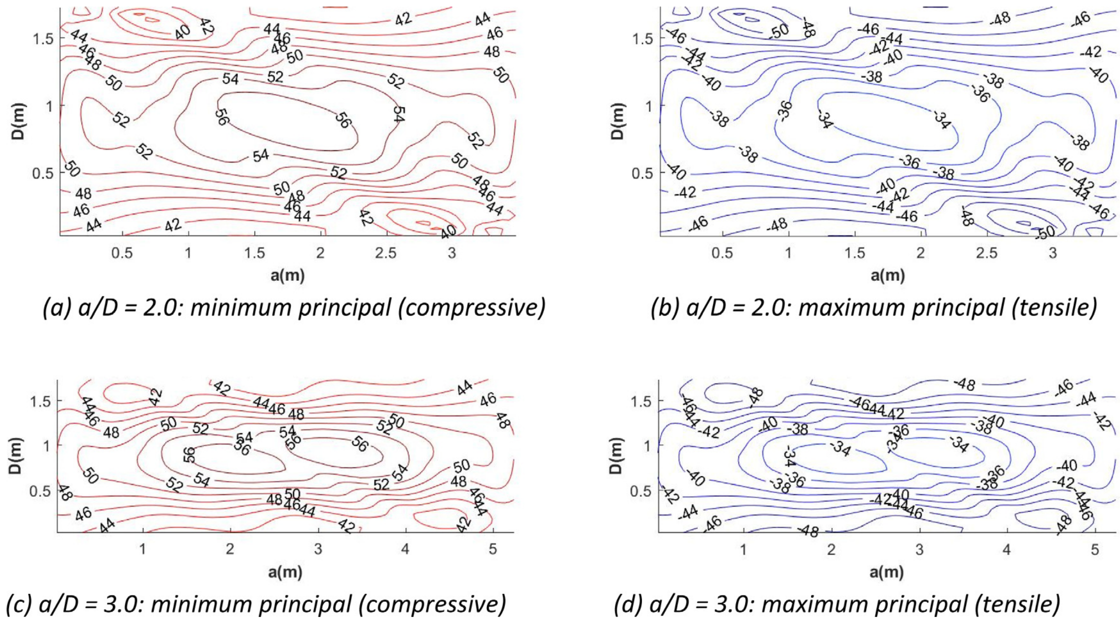

Fig. 20. Contour of angles of principal membrane stresses at V_u for AF-WF-PE models (center panel) with D/1000 imperfection and (a–b) $a/D = 2.0$ and (c–d) $a/D = 3.0$. Units of contours = degrees. Positive values signify counterclockwise rotation and negative values signify clockwise rotation from the horizontal.

- An imperfection study indicated that imperfections equal to or smaller than $D/1000$ exhibit similar shear performance (stiffness and strength), while $D/100$ imperfection slightly reduces these shear parameters. Further, the panel extensions boundary condition (i.e., continuity of the girder panel) appears to reduce sensitivity to imperfection magnitude.

An examination of initial imperfection magnitude indicated that $D/1000$ (which is on the order of measurements made at a fabrication shop [37]) enables shear postbuckling performance in FE models that correlates well with experimental data. Using the panel extension boundary condition with an initial imperfection magnitude of $D/1000$, a study of the load path of membrane stresses was performed on a realistic steel bridge girder panel with web depth 1.75 m, web slenderness 138, and panel aspect ratios of 1, 2, and 3. The following conclusions can be drawn from the load path study:

- At the top and bottom edges of the web, membrane stresses normal to the web edge are negligible at the ultimate postbuckling shear load V_u, and the flange stresses are correspondingly observed to be at less than 10% of the yield stress. Flanges reach yield only with significantly larger deflection beyond V_u. The flanges thus do not anchor substantial web membrane stresses up to V_u, and their engagement in a secondary postbuckling load path may develop following V_u.
- The horizontal membrane stresses normal to the vertical edge, where the stiffeners are located, are essentially zero if a panel extension is not modeled. The addition of panel extensions results in normal stresses on the vertical edges that are approximately 10% of the yield stress at V_u. Horizontal anchoring onto adjacent web panels can increase the ultimate postbuckling shear strength, though it is not necessary for the development of postbuckling shear strength.
- Compressive stresses parallel to the web panel edges (horizontal compressive stresses next to the flanges, vertical compressive stresses next to the stiffener) occur on the order of 10% of yield.
- Consistent with previous research [21–23,25,26], the vertical stiffeners carry a low level of axial load compared to the applied shear. Instead, the stiffeners are primarily engaged in bending as they provide lateral restraint to the web panel.
- Compressive membrane stresses redistribute and continue to increase after elastic shear buckling (V_{cr}), in some regions at a rate greater than before elastic buckling, contrary to tension field theories. These compressive membrane stresses increase more around the perimeter of the web and are greatest at the ends of the tension field (orthogonal to the tension field), where they exceed the corresponding tensile stresses.
- Though tension is significantly larger than compression at the center of the plate, the principal maximum (tensile) and minimum (compressive) membrane stresses are closer in magnitude around the perimeter of the plate (horizontal and vertical web edges).
- The von Mises stresses (based on membrane stresses) are highest at the ends of the tension diagonal, where both tension and compression stresses are large (up to 95% of the yield stress); however, considering bending, the von Mises stresses on the plate top and bottom surface of the web yield significantly on the tension diagonal due to second-order bending, the influence of which has been highlighted by the authors in previous work [20].

This paper recommends boundary conditions for the study of postbuckling shear mechanics and sheds light on the role of different girder components in the postbuckling shear behavior. A detailed study of the load path and stress distribution in the web highlights the interplay of tension and compression in the buckled web plate. The findings can be useful for code development for the design of each component in a plate girder and for enhancing the accuracy and mechanical correctness of shear strength models.

CRediT authorship contribution statement

Peter Y. Wang: Conceptualization, Methodology, Software, Validation, Formal analysis, Investigation, Data curation, Writing – original draft, Revised draft, Editing, Visualization, Project administration. **Parfait M. Masungi:** Methodology, Software, Validation, Formal analysis, Investigation, Data curation, Writing – Revised draft and editing, Visualization, Project administration. **Maria E.M. Garlock:** Conceptualization, Supervision, Resources, Writing – review & editing, Visualization, Funding acquisition, Project administration. **Spencer E. Quiel:** Supervision, Resources, Writing – review & editing, Funding acquisition.

Declaration of competing interest

The authors declare that they have no known competing financial interests or personal relationships that could have appeared to influence the work reported in this paper.

Acknowledgments

This research was sponsored by the National Science Foundation (NSF), United States under grants CMMI-1662886 and CMMI-1662964. All opinions expressed in this paper are the authors' and do not necessarily reflect the policies and views of the sponsors. The authors would like to acknowledge Ted P. Zoli for his consultation in this work.

References

[1] J.M. Wilson, On specifications for strength of iron bridges, Trans. Am. Soc. Civ. Eng. 15 (1) (1886) 401–403, 489-490.
[2] H. Wagner, Flat Sheet Metal Girder with Very Thin Metal Web, Tech. Notes. 604, 605, 606, National Advisory Committee on Aeronautics, Washington, DC, 1931.
[3] American Association of State Highway and Transportation Officials, eigthth ed., in: AASHTO LRFD Bridge Design Specifications, AASHTO, 2017.
[4] AISC, Specification for Structural Steel Buildings, American Institute of Steel Construction, Chicago, 2016.
[5] Eurocode 3: Design of Steel Structures: Part 1.2 General Rules - Structural Fire Design, BSI, London, 2001.
[6] D.W. White, M.G. Barker, Shear resistance of transversely stiffened steel I-Girders, J. Struct. Eng. 134 (9) (2008) 1437–1449.
[7] D.R. Hingnekar, A.Y. Vyavahare, Mechanics of shear resistance in steel plate girder: Critical review, J. Struct. Eng. 146 (6) (2020).
[8] O. Kerensky, A. Flint, The basis for design of beams and plate girders in the revised british standard 153, Proc. Inst. Civ. Eng. 5 (4) (1956) 427–440.
[9] K. Basler, B. Yen, J. Mueller, Web Buckling Tests on Welded Plate Girders, Vol. 64, Welding Research Council, 1960.
[10] K. Basler, Strength of plate girders in shear, Trans. ASCE 128 (2) (1961).
[11] S.C. Lee, C.H. Yoo, Strength of plate girder web panels under pure shear, J. Struct. Eng. 124 (2) (1998) 184–194.
[12] A. Selberg, On the Shear Capacity of Girder Webs, Univ. Trondheim Rep. Norway, 1973.
[13] E.H. Gaylord, Discussion of K. Basler 'strength of plate girders in shear', Trans. ASCE 128 (Part II) (1963) 712.
[14] T. Fujii, On an Improved Theory for Dr. Basler's Theory, in: IABSE 8th Congr. Final Rep., New York, 1968.
[15] D. Porter, K. Rockey, H. Evans, The collapse behavior of plate girders loaded in shear, Struct. Eng. 53 (8) (1975) 313–325.
[16] T. Höglund, Shear buckling resistance of steel and aluminum plate girders, Thin-Walled Struct. 29 (1) (1997) 13–30.
[17] A. Daley, D. Davis, D. White, Shear strength of unstiffened steel I-Section members, J. Struct. Eng. 143 (3) (2017).
[18] C. Yoo, S. Lee, Mechanics of web panel postbuckling behavior in shear, J. Struct. Eng. 132 (1) (2006) 1580–1589.
[19] P. Wang, K. Augustyn, A. Gomez, S. Quiel, M. Garlock, Influence of boundary conditions on the shear post-buckling behavior of thin web plates, in: Conference Proceedings of the 2019 SSRC Annual Stability Conference, St. Louis, MO, 2019.
[20] M. Garlock, S. Quiel, P. Wang, J. Alos Moya, J. Glassman, Postbuckling mechanics of a square slender steel plate in pure shear, AISC Eng. J. (2019).
[21] S.C. Lee, C. Yoo, D. Yoon, Behavior of intermediate transverse stiffeners attached on web panels, J. Struct. Eng. 128 (3) (2002) 337–345.
[22] S.C. Lee, C.H. Yoo, D.Y. Yoon, New design rule for intermediate transverse stiffeners attached on web panels, J. Struct Eng. 129 (12) (2003) 1607–1614.
[23] K.N. Rahal, J.E. Harding, Transversely stiffened girder webs subjected to shear loading - part 1: behaviour, Proc. Inst. Civil Eng. 89 (2) (1990) 47–65.
[24] K.N. Rahal, J.E. Harding, Transversely stiffened girder webs subjected to shear loading-part 2: Stiffener design, Proc. Inst. Civ. Eng. 91 (2) (1990) 237–258.
[25] J. Glassman, V. Boyce, M. Garlock, Effectiveness of stiffeners on steel plate shear buckling at ambient and elevated temperatures, Eng. Struct. 181 (2019) 491–501.
[26] Y.D. Kim, D.W. White, Transverse stiffener requirements to develop shear-buckling and postbuckling resistance of steel I-Girders, J. Struct. Eng. 140 (4) (2014).
[27] A. Ghadami, V. Broujerdian, Shear behavior of steel plate girders considering variations in geometrical properties, J. Construct. Steel Res. 153 (2019) 567–577.
[28] C. Scandella, M. Neuenschwander, K.M. Mosalam, M. Knobloch, M. Fontana, Structural behavior of steel-plate girders in shear, J. Struct. Eng. 146 (11) (2020).
[29] J.D. Glassman, M.E.M. Garlock, A compression model for ultimate postbuckling shear strength, Thin-Walled Struct. 102 (2016) 258–272.
[30] S.C. Lee, D.S. Lee, a.C.H. Yoo, Further insights into postbuckling of web panels. I: Review of flange anchoring mechanism, J. Struct. Eng. 135 (1) (2009) 3–10.
[31] Dassault Systemes, Abaqus 2017 documentation, 2017, [Online]. [Accessed 2019].
[32] P.Y. Wang, M.E. Garlock, T.P. Zoli, S.E. Quiel, Low-frequency sinusoids for enhanced shear buckling performance of thin plates, J. Construct. Steel Res. 177 (2021).
[33] P.Y. Wang, Characterizing the Shear Behavior of Slender Square Plates under Pure Shear Load, Princeton Printer, Princeton, 2018.
[34] S. Timoshenko, J. Gere, Theory of Elastic Stability, second ed., McGraw-Hill Book Company Inc, New York, 1960.
[35] CEN, Part 1-5: Plated structural elements, in: EN $1993-1-5$ (2006) (English): Eurocode 3: Design of steel structures, Brussels, 2006.
[36] A. Jha, Investigation of the Shear-Strength of Built Up I-Section Members Via Test Simulation A Master's Thesis, Georgia Institute of Technology, Atlanta, 2016.
[37] A. Gomez, Web Out-of-Straightness in Plate Girders: Methodology for Measurements and Effects on Shear Capacity, Princeton University, Princeton, 2020.
[38] A. Bergfelt, J. Hovi, Thin-walled deep plate girders under static loads, in: Proceedings of the IABSE Colloquium, New York, 1968.
[39] A. Kamtekar, J. Dwight, B. Threlfall, Tests on Hybrid Girders (Report 2), Cambridge University, Cambridge, 1972.
[40] K.C. Rockey, M. Skaloud, The ultimate load behaviour of plate girders loaded in shear, Struct. Eng. 50 (1) (1972) 29–48.
[41] H. Evans, K. Rockey, D. Porter, Tests on longitudinally reinforced plate girders subjected to shear, in: Proceedings of Conference on Structural Stability, Liege, 1977.
[42] R. Narayanan, K. Rockey, Ultimate load capacity of plate girders with webs containing circular cut-outs, Proc. Inst. Civ. Eng. 71 (3) (1981) 845–862.
[43] F. Sakai, T. Fuji, Y. Fukuchi, Failure Tests of Plate Girders using Large-Sided Models, Structural Engineering Report, University of Tokyo, Department of Civil Engineering, Tokyo, 1966.
[44] M. Grubb, R. Schmidt, Design example 1: Three-span continuous straight composite steel I-Girder bridge, in: Steel Bridge Design HandBook FHWA-if-12-052 Vol 20, FHWA, 2012.
[45] P.Y. Wang, M.E. Garlock, T.P. Zoli, S.E. Quiel, Low-frequency sine webs for improved shear buckling performance of plate girders, in: 20th Congress of IABSE, New York City 2019: The Evolving Metropolis - Report, New York, 2019.
[46] AASHTO/AWS D1.5M/D1.5.2010 Bridge Welding Code, sixth ed., AASHTO, Washington, DC, 2010.
[47] A. Reis, N. Lopes, P. Villa Real, Design of steel plate girders subjected to shear buckling at ambient and elevated temperatures: Contribution from the flanges, Eng. Struct. 152 (2017) 437–451.
[48] S.C. Lee, C.H. Yoo, Experimental study on ultimate shear strength of web panels, J. Struct. Eng. 125 (8) (1999) 838–846.
[49] M. Alinia, M. Shakiba, H. Habashi, Shear failure characteristics of steel plate girders, Thin-Walled Struct. 47 (2009) 1498–1506.
[50] O. Steinhardt, W. Schroter, Postcritical behavior of aluminum plate girders with transverse stiffeners, in: IABSE Rep of the Working Commissions, Volume– Band 11, Colloquium, Design of Plate and Box Girders for Ultimate Strength, London, 1971.